ALMA MATER STUDIORUM
UNIVERSITÀ DI BOLOGNA

Dottorato di ricerca in Scienze chimiche
Ciclo XXV

Settore concorsuale di afferenza: 03/A2
Settore scientifico disciplinare: CHIM/02

Oxygen: Problems and Solutions in Electrochemistry

Presentata da:
Luca Bardini

Relatore:
Prof. F. Paolucci

Contents

Introduction

It is an interesting quirk of modern technological development[1] that most of the problems humans have to face are problems they have created themselves in the first place. And when it comes to applied science, oxygen is often at the center of the stage. No matter what field of chemistry one examines, oxygen is possibly the only element which is invariably either the solution to the chemists' troubles or one of the main challenges to face. At times, these two aspect can also occur simultaneously. Take organic chemistry, where achieving a controlled oxidation of organic compounds with molecular oxygen would be one of the major advances towards less environentally detrimental synthetic processes, while on the other hand oxygen is probably the major source of degradation of organic compounds, be them pharmaceuticals, dyes, polymers or more or less anything that comes to mind. Materials science brings other examples of the dual nature of oxygen: it is one of the most promising candidates for a relatively more sustainable energy production framework (i.e. fuel cells), and at the same time one of the major obstacles to face when developing photovoltaic cells. It is a major constituent of ceramic materials, which see applications in fields which vary from frying pans, to fuel cell electrodes and insulating panels for spacecrafts, while at the same time being one of the major players in the failure of metals and metal alloys. A similar situation is present in biochemistry, where oxygen is one of the essential building blocks that allow all aerobic organisms to go about their daily business. At the same time, however, oxidative stress is an important source of malfunctions in the metabolism of cells. In this respect oxygen looks like a perfect example of the insight of Philip von Hohenheim (a.k.a. Paracelsus) when he stated: "Alle Dinge sind Gift, und nichts ist ohne Gift. Allein die Dosis macht, das ein Ding kein Gift ist".[2]

[1] It order not to stray too far from the topic of the thesis the discussion is restricted to technology. This aspect is actually part of a very general attitude that can be spotted more or less unchanged in many aspects of human daily life

Of course, there is really nothing ambiguous or ambivalent in the nature of oxygen: it is an oxidant, and one that makes up a large portion of the atmosphere we live in. The difficulty to come to terms with the fact that everything that can be oxidized will, sooner or later, be oxidized, is merely one of the many examples that highlight the inability of human beings to adapt to the surrounding environment, in a frantic struggle to adapt the environment to themselves. Being oxygen one of the most abundant elements on earth it is only natural that it will be often encountered within these struggles, at times as friend, at times as foe.
In this thesis practical experimental examples are employed to outline the different aspects of oxygen as they are encountered in electrochemistry, that is:
Destruction by oxygen - The corrosive effects towards metals that the oxidative nature of oxygen can cause are first examined via the description of the dissolution of copper in the presence of a primary amine: allylamine. It will be shown that allylamine and oxygen play a complementary role, and are therefore both needed for the corrosion process to proceed.
Protection from oxygen - The development of a passivating film for the protection of a surface from the oxidative action of oxygen is described: the film is the result of the electropolymerization of mixtures of allylamine and diallylamine on glassy carbon.
Consumption of oxygen - The third chapter will shift towards a biologically oriented application of catalysis: a carbon nanotube based oxygen reduction catalyst is studied, which could prove useful in the detection of oxygen in biological media.
Generation of oxygen - Finally, the generation of oxygen via a carbon nanotube based water oxidation catalyst is presented as an example of the effectiveness of a new hydrogel as a dispersing medium for highly insoluble carbon nanotubes.

[2]Everything is poison, and nothing is without poison. It is only the dosage that makes it so that something is not a poison.

Chapter 1

Corrosion of Copper by Allylamine and Oxygen

Contents

It is known that copper is normally covered by an oxide film at ambient conditions; this oxide film protects it from humidity and air, preventing further oxidation and making it relatively corrosion resistant. The presence of atmospheric pollutants (most notably sulfur oxides) or salts in humid environments (such as sodium chloride in coastal areas) decrease its resistance due to the attack of the surface oxide and the formation of copper chlorides and sulfates. This process, however, usually takes a relatively long time (months or even years). The effect of the above mentioned corrosion can, however, be seen with the naked eye without difficulty: the oxides of copper have, in fact, an easily recognizable black (cuprous oxide) and red (cupric oxide) color. Copper sulphate, copper chloride and copper carbonate hydrated complexes are green/blue, and can be easily spotted on the surface of many older bronze sculptures.
In this chapter another class of molecules which causes copper to corrode, apparently much faster than in the previously mentioned cases, is identified in primary amines. When it comes to corrosion, the relationship between copper and amines in the literature is cloudy at best. Nitrogen is known to bind to copper, as evidenced by the literature on complexes of copper and nitrogen ligands[1], and many amines are generally found to be corrosion inhibitors, as evidenced by the presence of works in the scientific literature describing the protective effects of various kinds of amines towards copper dissolution in aggressive media [2, 3] some even arguing that a higher amine

concentration increases the inhibiting power of the solution [4]. On the other hand, there are various reports concerning the corrosiveness of amines towards copper [5, 6, 7]. Two deciding factors which seem to draw the line are the presence of oxygen and the concentration of the amine. This study is focused on the corrosion of copper by allylamine.

1.1 Experimenal Section

In all experiments the corrosive solution used was 0.1M allylamine in water. The concentration of allylamine was adjusted so that an advanced stage of the corrosion process could be reached within 48 hours from the start of the experiment; this condition was necessary due to logistic constraints in our laboratory.
Copper plates 2cmx1cm in size were employed for all electrochemical and Raman experiments. Before use each plate was sonicated in ethanol for 3 minutes. All impedance experiments were carried out with a BIOLOGIC potentiostat. Cyclic voltammetries in anhydrous conditions were performed using home-made anhydrous acetonitrile on a home-made vacuum line with Amel mod. 568 function generator and a Nicolet 3091 oscilloscope.

1.2 Optical Analysis

A picture of a copper platelet after prolonged exposure to allylamine is provided in Figure 1.1. Three areas, indicated by the dots, can be easily spotted: (A,B) the area of the platelet immersed in solution, (C) the interphase between water and air and (D) the area of the platelet exposed to air. A visual analysis already reveals the presence of black cupric oxide in the submerged portion of the sample and at the water-air interface, while green deposits (point D) are present in the upper part of the plate, signalling the likely presence

of copper complexes: green deposits are, in fact, commonly found on copper and copper alloys exposed to air, and are usually due to copper chlorides and copper sulfates or sulfides. The area marked as

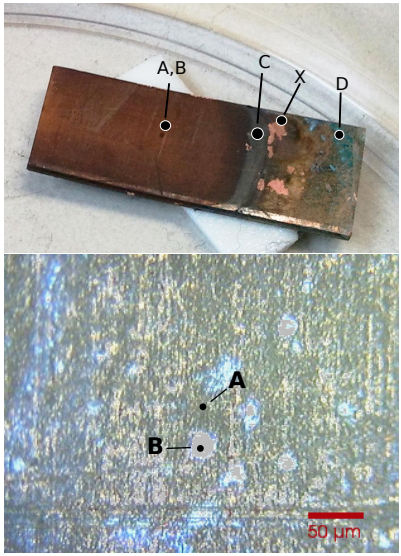

Figure 1.1: Top: copper plate after 72 hours of exposure to a 0.1M allylamine solution. Three distict areas can be spotted: dot A,B is on the part of the plate which was immersed in the solution, point C marks the black solution/air interphase while point D in on the plate which was in air. Bottom: Optical image of the portion of the copper plate immersed in the corrosive solution at points A,B

point (X) shows a region of the sample in which the deposits have been accidentaly removed during the cleaning of the sample after its removal from the corrosion cell. The fact that a weak flow of argon was sufficient to displace the corrosion products is an indication of their fragility and of the ease with which the corrosive medium can infiltrate under the deposits and continue dissolving the substrate. A

closer inspection with an optical microscope reveals that the surface of the sample is more varied than appears at the naked eye. In the lower part of Figure 1.1, it can be seen how amidst the black deposits on the sumberged portion of the platelet, white deposits are present. To more precisely identify the chemical species present on the substrate Raman spectroscopy was run in collaboration with Dr. Alessia Scarsi from the group of prof. M. Meneghetti at the University of Padua, IT. All spectra shown in Figure 1.2 were obtained using Renishaw inVIA Raman microscope with an excitation wavelength of 633nm with ca. 1.4mW incident power on the surface at 20x magnification with a 30s acquisition time. Measurements were conducted after 24, 48 and 74 hours of immersion in a 0.1M acqueous allylamine solution.

The main features in the spectra is two peaks at 625cm^{-1} and 525cm^{-1}. The peak at 625cm^{-1} is characteristic of both CuO and Cu_2O[8], while signals specific of CuO are found at lower frequencies: $Cu(OH)_2$ shows in fact a band at 490cm^{-1}, which together with the shoulder at 525cm^{-1} has been connected to CuO. Nothing can be said on the stoichiometry of the oxide layer, however, the relative intensity of the two bands varies depending on the region of the copper plate where the spectrum is recorded, showing a general prevalence of Cu_2O except in region A, where either a prevalence of CuO or a more balanced mixture of cupric and cuprous oxide seems to be present. The intensity of the 525cm^{-1} peak also diminishes significantly over time, regardless of the position on the plate: this suggests that as the corrosion advances either the amine brings Cu(II) species in solution as soon as they are formed, or allylamine complexes Cu(I) before it is oxidized to Cu(II) by oxygen. In both cases allylamine acts as a complexing agent which speeds up the attack of oxygen on copper, rather than participating in the redox reactions at the surface. As can be seen in Figure 1.2 spot A shows two distinct peaks at 1350/1600cm^{-1} while spot B and on the interphase at spot C the signals are weaker, with a prevalence of the feature at 1200cm^{-1}. All these peaks have been assigned to bending motions of the amine group[9] and are consistent with the adsorption of allylamine on the

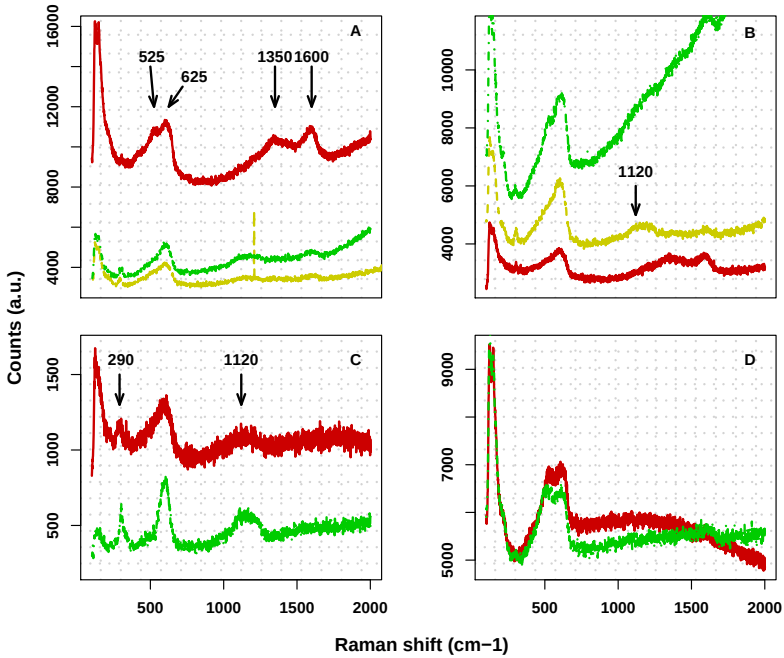

Figure 1.2: Raman spectra of different areas of the copper samples exposed to the acqueous allylamine solution for 24 hours (red), 48 hours (yellow) and 72 hours (green). The labels A,B,C and D refer to the ares indicated in the images shown in Figure 1.1

oxide surface. At lower frequency a peak at 290cm^{-1} is clearly visible at the interphase (Figure 1.2C) and on the submerged portion of the plate at longer times (green and yellow traces in Figure 1.2A-B). This feature has been previously described as the vibration of the Cu-Cl bond[8], while a similar feature at 287cm^{-1} has been assigned to ν(Cu-N)[9]; in the present case, being allylamine the only

species in solution, it can be taken as a signal of the presence of a Cu-allylamine bond. Although care should be taken in giving quantitative significance to the intensity of Raman peaks, it would seem like the Cu-N signal is strongest at the interphase: this fact could easily be explained by noting that in the submerged regions of the plate the water soluble Cu-allylamine complex would be rapidly be hydrated and brough into solution, while at the air-water interface a higher build-up of the deposits could take place thanks to a slower dissolution.

1.3 Electrochemical Analysis

The corrosion of copper was at first followed by recording impedance spectra at 2 hour intervals in the range 1MHz-10mHz. The cell set-up was as follows: the copper platelet was used as the working electrode, connected to a platinum counter electrode and an Ag/AgCl reference electrode. To model the EIS spectrum obtained roughly 1 minute (0.017 hours in Table 1.1) after the addition of allylamine an equivalent circuit with a resistor in series to two parallel constan phase element (CPE)/resistance couples was used (Figure 1.3:Top); already at two hours after the addition of allylamine, however, it was necessary to include a third parallel capacitance/resistance element (Figure 1.3:Bottom). Other equivalent circuits proposed in the literature were tested[10, 11], but resulted in higher fitting errors as evidenced by higher χ^2 values. The results of the fitting of the impedance spectra are reported in Table 1.1, while a typical evolution of the phase angle in the is reported in Figure 1.4. The phase angle spectrum of copper in water showed a peak at low frequency, which can be seen in the spectrum recorder immediately after the addition of allylamine (□), together with a characteristic high frequency peak. After one hour (•) the high frequency feature has shifted to frequencies >1MHz (only a tail remains visible), while two peaks are now present at low frequency, at approximately 1Hz and 80Hz respectively. A comparison with analyses of similar systems

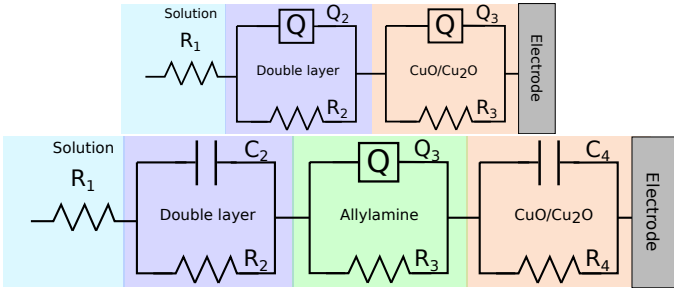

Figure 1.3: Equivalent circuits used to model the impedance spectra at 1 minute (Top) and 2 hours and beyond (Bottom) after the addition of allylamine.

in the literature allows to assign the high frequency peak to double layer charging and the low frequency peaks at adsorption/desorption processes[12]. In the present case the 1Hz peak is likely due to copper ions in the oxide film present on the surface, while the 80Hz peak, which appears after the addition of allylamine and gradually becomes predominant, is likely due to allylamine. The increasing phase angle of the copper related peak might hint to a thinning of the oxide layer, which gradually reaches a steady state when copper oxidation is balanced by Cu(II)/Cu(I) dissolution by allylamine. The changes in the values of the capacitances and CPEs over time follow the pattern outlined by the phase angle, with the sharp increase in Q3 (allylamine adsorption) mirrored by the sharp decrease in C4 (oxide film thinning) from 2 to 4 hours after the addition. The resistances exhibits a more oscillatory behavior, which might reflect the oxide formation-oxide dissolution phases of the corrosion process, although it is not possible to quantitatively link the two without further in-situ studies (i.e. in-situ x-ray or raman analysis). Another sign of the ongoing corrosion process is the dropping of the solution resistance to 0Ohm as more ions are driven in solution.

A test was conducted to gain experimental evidence that both ally-

Table 1.1: Fitting of impedance spectra measured at different time intervals after the exposure of a copper plate to allylammine in water. The spectra are shown in Figure 1.4. Measurement Units are omitted for clarity[a]

Hours	0.017	2	4	12	14	20
R1	46.5	0	0	0.4	0	1.5
R2	328	170.4	900	111274	12101	154714
Q2[b]	$17{\cdot}10^{-9}$	$3{\cdot}10^{-9}$	$21{\cdot}10^{-6}$	$98{\cdot}10^{-6}$	$7{\cdot}10^{-6}$	$83{\cdot}10^{-6}$
a2	0.98	-	-	-	-	-
R3	66240	50758	239754	33765	205505	52802
Q3	$64\cdot10^{-6}$	$1{\cdot}10^{-4}$	$65{\cdot}10^{-6}$	$11{\cdot}10^{-6}$	$29{\cdot}10^{-6}$	$10{\cdot}10^{-6}$
a3	0.78	0.66	0.68	0.77	0.66	0.80
R4	-	59375	127	211	236	244
C4	-	$3{\cdot}10^{-4}$	$3{\cdot}10^{-9}$	$1{\cdot}10^{-9}$	$1{\cdot}10^{-9}$	$1{\cdot}10^{-9}$

[a] All resistances (R*) measured in Ohm, all true capacitances (C*) measured in Fahrad, all contant phase elements (Q*) measured in $F \cdot s^{a-1}$.

[b] For all spectra besides 0.017, a true capacitance was used

lamine and oxygen are both needed in order for corrosion to occur, as the former by itself would not be able to oxidize metallic copper once the oxide layer has been removed. A copper plate was left in a 0.1M allylamine solution with acetonitrile as the solvent. A silver wire pseudo electrode and a platinum counter electrode were also assembled in the cell. The choice of solvent followed from the availability of self-made highly anhydrous and oxygen-free acetonitrile in our lab. The solution was left under vacuum (10^{-6}bar) for 7 days without registering any visible signs of corrosion. Subsequent voltammetries in the range -0.5-0.5V showed no signs of oxidized copper species.
To further the analysis of the influence of oxygen on the process a voltammetric investigation of the behavior of copper in a 0.1M allylamine acetonitrile solution was run. A copper plate was left in the solution in an air tight cell until the solvent took a faint blue color (ca. 5 hours), indicating that the corrosion process had begun. Voltammetric experiments were then carried at first after carefully

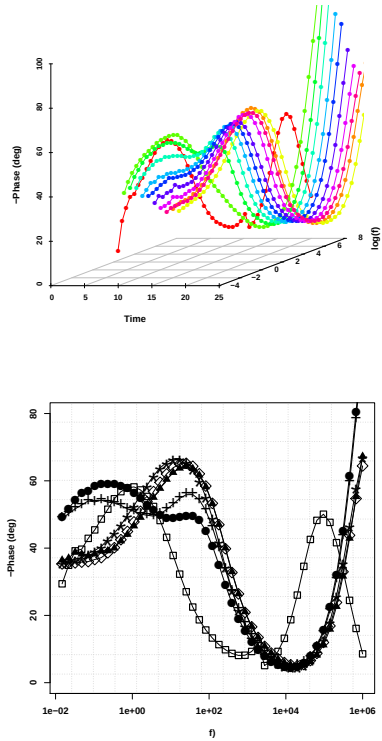

Figure 1.4: Top: three-dimensional plot of the phase angle over a 24 hours timespan. Phase angle spectra were recorded at circa 2 hour time intervals. Bottom: phase angle plots at ¡1 minute (□), 2 hours (•), 4 hours (+) , 12 hours (Δ), 14 hours (◊) and 20 hours (⋆) after the addition.

removing air from the cell with argon and then after letting oxygen back into the cell (red curve to black curve). The results graphed in Figure 1.5 show the presence of copper(II) accumulation and stripping peaks (red arrows) [13, 14] in the voltammograms recorder in the presence of oxygen. These peaks are not present in the absence of oxygen and their area increases in time after oxygen has been let into the cell. The peaks pertaining to the redox process of copper(I)

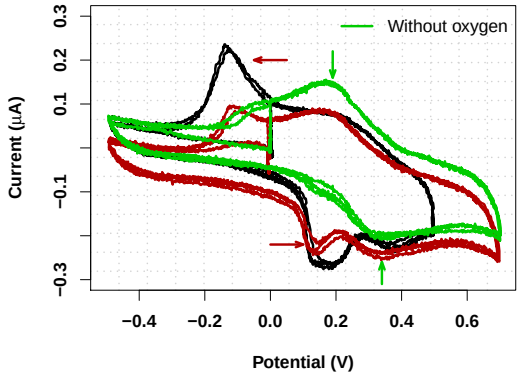

Figure 1.5: Voltammetric measurements of the surnatant solution after 5 hours of corrosion of a copper plate in 0.1M allylamine in acetonitrile. The voltammetries were recorded after careful deaeration (green) and after 10 (red) and 30 minutes (black) from the re-oxygenation of the solution. Working electrode: 10μm Pt. Reference Electrode: silver wire. Counter electrode: platinum wire.

in solution are present both with and without oxygen (green arrows). This pair of peaks has been assigned to free (hydrated) Cu(II) ions [15], but the redox potentials of copper ions can vary only slightly upon complexation if the ligand is electrochemically inactive[16, 17]; it is therefore not possible to unambiguously state whether copper leaves the surface as an acquo-ion, an amino-complex or, maybe more likely, a hydrated amino complex.

1.3.1 Tentative Corrosion Mechanism

From the data described so far a plausible reaction mechanism can be outlined:

$$Cu \xrightarrow{O_2} CuO + Cu_2O \xrightarrow{H_2NR} Cu(NR)_x(OH)_y \quad (1.1)$$

This scheme tries to include the evidence obtained from both previous works present in the literature, and the experimental data gathered in this work: 1) the corrosion does not procede in the abscence of oxygen; 2) there is evidence of a depauparation of CuO from the corroding surface over time; 3) at exposure times $\geq$24 hours signals of direct Cu-N bonding are present. The exact mechanism with which the amine attacks the copper oxide cannot be determined with the data in our possesion, as the oxidation state of copper when it leaves the surface after the attack of allylamine. It can be speculated, however, that the possible release of an acidic proton from allylamine as the copper complex is formed might lead to a local pH decrease which could further enhance the dissolution process by catalyzing the reduction of oxygen and subsequently impeding the formation of a new surface oxide layer[18] as outlined in the reaction shown below

$$2Cu + O_2 + 4H^+ \rightarrow 2Cu^+ + 2H_2O \quad (1.2)$$

Furthermore, the possibility of a direct oxidation of metallic copper by the copper-amine complex already gone in solution has already been described in the literature in the case of ammonia [10], adding to the potential corrosiveness of allylamine.

1.4 Conclusions

The corrosiveness of concentrated acqueous solutions of allylamine towards copper has been attested and studied with both electrochemical (EIS,CV) and optical (RAMAN) techniques. The experimental data gathered point towards a synergic effect between oxygen and allylamine, where oxygen acts as the oxidizing agent while allylamine

acts as the ligand which brings copper in solution and prevents the formation of a passivating oxide film.

Acknowledgements

Alessia Scarsi
Università degli Studi di Padova
Dipartimento di Scienze Chimiche
Via Marzolo, 1, 35131 Padova

Raman measurements.

Moreno Meneghetti
Università degli Studi di Padova
Dipartimento di Scienze Chimiche
Via Marzolo, 1, 35131 Padova

Head of the photonics research group.

Chapter 2

Passivating Properties of Electropolymerized Allylamine co-Polymers

Contents

The field of surface functionalization is a multi-faceted one. Researchers want to modify surfaces for rather opposite purposes: either they want to make a surface more reactive (and often selectively reactive towards a particular molecule or class of molecules) or they want to render it completely unreactive. It is a rather funny quirk of modern technology that when the physical properties of a material seem just right to solve a particular task, its chemical properties will likely turn out to be less than optimal for the task, and viceversa. This seems to be especially true when it comes to metals. The fact that, with very few notable exceptions, no metals in their reduced form can be found in nature, is a not so subtle hint to the fact that whenever one is going to put a metallic material in contact with the environment (air and humidity and salts and the diverse anthropogenic substances present in our modern cities) he or she will create a thermodynamically metastable situation at best. In other words: it is just a matter of time before the metal(s) will return to their native oxide form. Some metals have an effective self-defense mechanism that can slow this process down considerably in the spontaneous formation of a compact and impermeble surface oxide, copper being a notable example. This strategy works only provided that there are no other molecules other than oxygen and water. In the case of copper, the presence of chloride anions or sulfur oxides will transform

the surface oxide to copper chloride and copper sulfates of sulfide respectively. The porosity and brittleness of these surface layers will leave the underlying metal exposed to further oxidation until complete dissolution or failure of the metallic component.
Chapter 1 showed how allylamine is another such molecule, which in the presence of oxygen leads to the premature demise of a surface. It will be now be shown how that synergy can be reversed by using the same molecule (allylamine) to form polymers which screen a material from the environment, thereby impeding the corrosive action of oxygen instead of aiding it.
Allylamine olygomers have long been know to chemists; up to now, they have been obtained primarely by polymerization initiated either with initiators after γ- or UV-irradiation[19] or plasma processing[20], the former commercially available as an oligomer solution, the latter deposited on the substrate of interest and covalently attached to the surface via the plasma process. The positive charge of the deposited films has been successfully employed to favor cell and macromolecule (i.e. proteins, nucleic acids) adhesion[21, 22].
In this chapter it will be shown that allylamine can also be polymerized electrochemically, bypassing the need for complex instrumentation, initiators and ionizing radiation; it will also be demonstrated that films with superior charge transfer resistance can be obtained by mixing equimolar amounts of allylamine and diallylamine in the reaction mixture.

2.1 Experimental Section

The experimental setup used for the polymerization of allylamine films is oulined in Table 2.1. Allylamine was obtained from Aldrich. Polymerization and permeability tests were conducted in acetonitrile (Aldrich >99%). The supporting electrolyte was in all cases tetrabutylammonium tetrafluoroborate ($TBABF_4$). Glassy carbon disk electrodes (Sigradur G, HTW,Ø=1mm) were used for all electrochemical experiments, while 1cm×1cm×1mm glassy carbon plates

Table 2.1: Experimental setup for the electrochemical cell and the solution used in the electropolymerization of allylamine

Solution		
[Allylamine]	**Solvent**	**Electrolyte**
10mM	Acetonitrile	$TBABF_4$ 0.1M
Electrodes		
Working	**Counter**	**Reference**
Glassy Carbon [a]	Pt wire	Ag/AgI

[a] Glassy carbon rods with a disk diameter of 0.5cm were used for the voltammetric and impedance analysis, while 2cmx2cm glassy carbon plates were employed for the XPS and AFM analysis.

(Sigradur G, HTW) were employed for ellipsometric and XPS measurements. A CH Instruments 660B potentiostat was used for all electrochemical experiments. AFM analysis was carried out with Digital Nanoscope 3D multimode microscope (Veeco) using phosphorous N-doped silicon probes (spring constant 20-80Nm^{-1}, resonance frequency 250-300kHz, nominal tip radius ¡ 10nm) operating in tapping mode. XPS experiments and analysis were perormed by M. Ceccato at Aarhus University using a Kratos Axis Ultra-DLD instrument witha monochromatic Al Kα X-ray source at a power of 150W, and the CasaXPS software respectively. Ellipsometry was performed with a rotating ellipsometer by Dre (DE), at a measurement angle of 65°.

2.2 Polymerization of Allylamine

The deposition of the polymer onto the glassy carbon (GC) surface was done with 5 consecutive cyclic voltammetries performed at a scan rate of 10mV/s (Figure 2.1).

The possibility to deposit the layers at faster scan rates was also

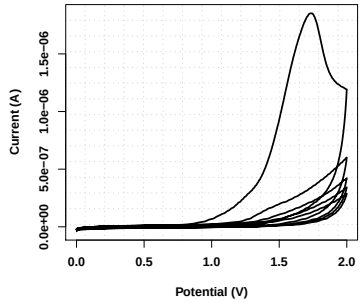

Figure 2.1: 5 consecutive cyclic voltammetries at 10mV/s showing the deposition of the allylamine polymer and the subsequent passivation of the electrode surface.

explored, resulting in reproducibly inferior blocking properties of the films; increasing the number of cyclic voltammetries did not improve the behavior of the layers.

2.2.1 Blocking Properties

After electropolymerization the electrode was briefly sonicated in acetonitrile and rinsed with acetone. It was then placed in a solution of 2mM ferrocene in acetonitrile with 0.1M $TBABF_4$ as the supporting electrolyte. The counter electrode was a platinum wire, while Ag/AgI was chosen as the reference electrode. In Figure 2.2 the results of these tests are given. The cyclic voltammetry at the GC after deposition of the layers (solid line) show a strongly suppressed electron transfer. Electrochemical impedance spectroscopy was performed in the same solution at OCP in the frequency range 10mHz-100kHz with a 2mV amplitude, The EIS spectrum shows signs of redox activity; these can be spotted in the Bode plot presented in the right graph in Figure 2.2 as two sigmoids in the absolute value of

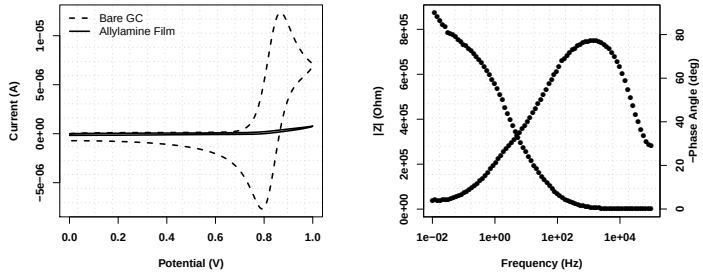

Figure 2.2: Left: voltammetry of ferrocene in acetonitrile at a clean (- - -) and filmed electrode (—), showing the passivation of the electrode surface by the polyallylamine layer; Right: Bode plot of the filmed electrode.

the impedance and as a weak capacitive contribution between 1Hz and 10Hz visible in the phase angle.
The impedance data were fitted with a Randles circuit with a constant phase angle element (CPE) in place of the capacitor: this substitution is necessary in order to take into account the fact that the phase angle has its absolute maximum at -80° instead of the -90° expected for an ideal capacitor, which has been linked to high surface roughness of glassy carbon [23]. A charge transfer resistance of $8.4 \cdot 10^5 \Omega$ was calculated from the impedance plot. This could indicate a very thick film, but the film thickness measured by ellipsometry and included in 2.2 is only 10nm. The resistivity of the GC-A_{argon} film is therefore higher than for most other grafted films: values in the $10^4 \Omega$ range have been in fact reported for highly fluorinated, hyperbranched polyacrylic acid polymers in the presence of $Fe(CN^{3-/4-})$ [24] as well as for polyallylamine-polystyrenesulfonate polyelectrolyte films, also with ferro/ferricyanide as the redox probe [25]; this difference is all the more significant considering that the heterogeneous rate constant for the oxidation of ferrocene is significantly higher than that of the ferro/ferricyanide couple.[26, 27]
Despite the high charge trasfer resistance, the defects previously

noted in the voltammetry and Bode plot of Figure 2.2 cause a progressive swelling of the polymer which allows increased diffusion of ferrocene to the electrode.

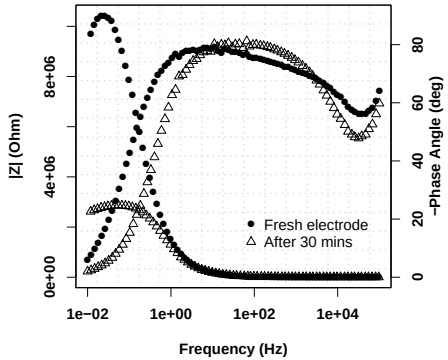

Figure 2.3: Bode plots of a freshly deposited allylamine film (•) and a film after 30 minutes of immersion in acetonitrile (Δ)

This can be seen in Figure 2.3, where a reduction of the blocking properties of the films after 30 minutes of immersion in acetonitrile is evident from the sharp decrease in the absolute value of the impedance and from the narrower region in which capacitive behavior is displayed.

2.3 Polymerization of Composites

In order to make the films more compact and stable against solvent swelling addition of a cross-linker as diallylamine to the reaction mixture was investigated, while keeping the structure and composition of the films as unchanged as possible. Experiments were performed

at different allylmine-diallylamine ratios, while keeping the cell setup described in Table 2.1. The R_{CT} for the 1:10 copolymer film is 44MΩ which is almost 80 times larger than for the allylamine film (Figure 2.4 and Table 2.2).

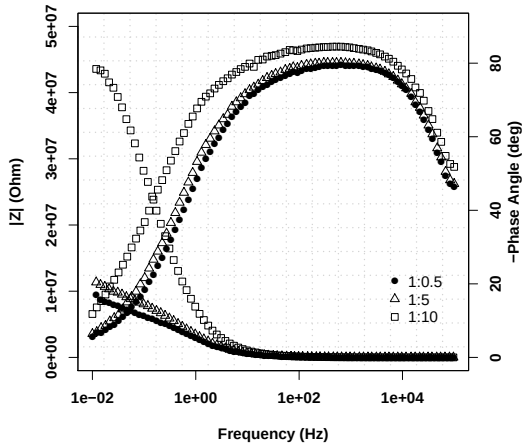

Figure 2.4: Impedance spectra of films deposited from solutions with different allylamine-diallylamine ratios: 1:0.5 •; 1:5 Δ; 1:10 □. The ratios 1:1 (not shown) and 1:10 give almost superimposable spectra

Most remarkably, this large increase in R_{CT} takes place with no increase in film thickness as found in Table 2.2. The polymer film deposited from diallylamine solutions without allylamine has blocking properties similar to those of allylamine films. Experiments conducted at higher allylamine concentrations without diallylamine also show that the increase in charge transfer resistance due to an increase in monomer concentration is much more contained than that caused by the presence of both allylamine and diallylamine. These facts indicates that the increase in passivating character of the copolymer

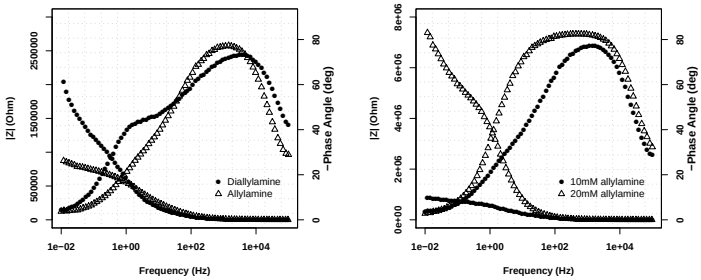

Figure 2.5: Left: blocking properties of an allylamine only (Δ) and a diallylamine only ($\bullet$) film. Right: Effect of a higher concentration of monomer on the impedance of the films. The spectra of a film deposited from a 10mM ($\bullet$) and a 20mM (Δ) allylamine solution are shown.

films is due to a synergyc effect present when both allylamine and diallylamie are present in the reaction mixture (Figure 2.5). To gain further insight into the mechanism of the deposition, impedance and AFM measurements were performed after 1,3 and 5 CV cycles. The AFM images shown in Figure 2.6 suggest that the deposition of the films takes place in a layer by layer fashion that does not seem to involve the formation of islands but, rather, of a uniform film already after the first scan. The surface roughness measured by AFM shows little variation and remains around 3nm until after 4-5 CV cycles, after which it decreases to 1.7nm. The morphology of the film appears to be well-ordered and aligned polymer chains. The XPS results show a high oxygen content of 12% is present in both allylamine and copolymer films created under aerated conditions. The most significant difference is, however, the C:N ratios; the latter are significantly higher for the copolymer, as expected by the incorporation of diallylamine, which contains more carbon atoms. For the copolymer film at 20° the C:N ratio is 4.0, whereas at the same angle it is only 3.1 for the allylamine film. From the increase of 0.9 it can

Table 2.2: Charge transfer resistance R_{CT} constant phase element values (Q) and frequency power (n) obtained from impedance spectra for grafted allylamine with and without oxygen and co-polymers with and without oxygen deposited from a 1:10 allylamine/diallylamine mixture onto GC [a]

Film	d (nm)	$R_{CT}/10^6\Omega^a$	$Q/10^{-8}S \cdot sec^a$	n
Allylamine + O_2	9.3 ± 0.9	0.84	3.2	0.92
Allylamine - O_2	10.0 ± 0.4	66 ± 4	5.02	0.84
Copolymer + O_2	9.8 ± 0.6	44.4 ± 1	2.2	0.92
Copolymer - O_2	10.5 ± 0.2	75.0 ± 6	3.9	0.84

[a] Impedance spectra were fitted with a modified Randles circuit with a constant phase element in place the capacitance

be inferred that the main component of the film (67% molfraction) remains polymerized allylamine, and about 33% of the film is made up by diallylamine. This result is quite significant since the grafting solution contained allylamine and diallylamine in a 1:1 ratio, and it shows that the polymerization ratio for the AD-copolymer is not random.

The C:N ratio at 50° and 90° take-off angles are 4.0 and 4.2 respectively, but, especially for the latter, some contribution to the %C from the GC surface is to be expected. This is supported by the C1s core-level spectra shown in Figure 2.7 for the three take-off angles 90°, 40° and 20°. It is evident that the main difference between the 90° spectrum and the other two is the lack of a component with a low and sharp binding energy profile at 284.4eV, which is the characteristic for the C1s in the GC surface. The C1s core-level spectrum (Figure 2.7) recorded at 90° take-off angle has been fitted with 5 components: a first peak at 284.4eV (C=C) is assigned to sp^2 hybridized carbon mainly originating from the GC substrate. The peak at 285eV relates to aliphatic carbon (C-C) while the signal at 286.6eV corresponds to carbon atoms bound to an amine, imine or oxide/hydroxy groups (C-N, C=N and C-O). A fourth component

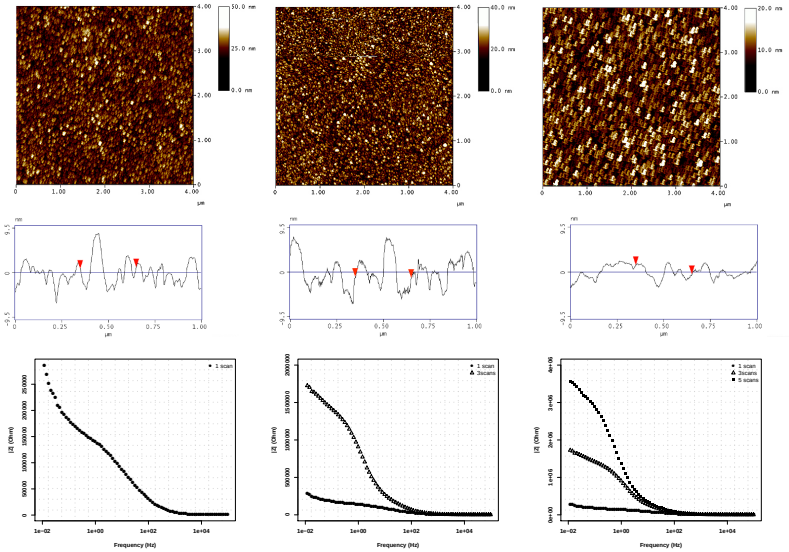

Figure 2.6: From left to right: AFM images of a 1:10 allylamine-diallylamine co-polymer recorded after deposition with 1, 3, 5 cyclic voltammetries; RMS values are 3.4nm, 3.1nm and 1.7nm respectively. From top to bottom in each column: morphological image, cross section of the morphological image and absolute impedance recorded in a 2mM ferrocene solution.

at 288.0eV is assigned to carbonyl groups (C=O) and amide bonds (N-C=O)[28].

2.3.1 Considerations on the Polymerization Mechanism

Despite the number of works related to the electrochemical properties of amines, to the best of our knowledge no material seems to be present on the electrochemical properties of allylamine. De-

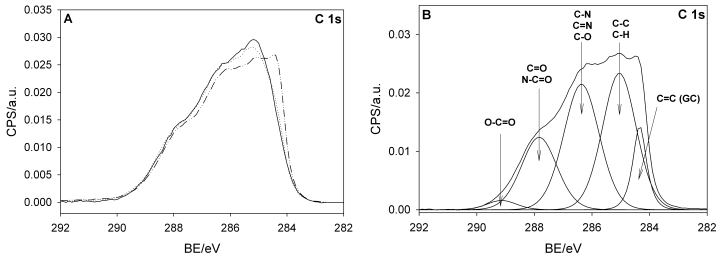

Figure 2.7: Core-level spectra at GC plates modified by 5 consecutive cyclic voltammograms in 0.1M $TBABF_4$ in ACN containing 10mM allylamine and 10mM diallylamine using a sweep rate of 10mV/s in an open cell (air). A: C 1s core-level spectra recorded at different angles: 90° (− · −),40° (· · ·) and 20° (−). B: deconvolution of C 1s core-level spectrum recorded at 90°.

spite the lack of direct experimental data, inferences can be made regarding the mechanism of polymerization by analogy with related reactions described in the literature. The possibly closest example is the plasma polymerization of allylamine, described by Choukourov et al. [29]; the process is therein described as forming polymer chains perpendicular to the substrate, the reactive species being radicals centered on nitrogen or on the adiacent carbon after detachment of an aminyl radical as a consequence of the ion bombardment, the latter process being favored at higher RF power as evidenced by the relative concentration of primary and secondary amines, the ratio approaching at 20W.
Caution is needed, however, since in the case of plasma synthesis polymerization can only happen on the substrate, while in the electrochemical case homogeneous reactions cannot be ruled out. In this context, it has been long known that amines can be electrochemically oxidized, allylamine, as previously shown, being no exception. Their behaviour in the presence of a glassy carbon surface has also been studied in the classic work of Deinhammer et al.[30] in which

it was proven that oxidized amines can graft onto the electrode surface. This is also expected to happen in the present case; however, the presence of a double bond on allylamine also opens other reaction pathways, such as an addition of the nitrogen radical to the double bond. The kinetics of addition of aminium radicals on olefines have been thoroghly studied [31], demonstrating how the reaction readily takes place in acetonitile at STP. The two processes not being mutually exclusive, it is likely that the polyerization reaction procedes both via a grafting onto the substrate as well as in solution. The carbon radical generated by the attack of the nitrogen radical on the double bond should also participate in the reaction, being itself able to readily attack olefins [32, 33]. The situation is further complicated by the possibility of an intramolecular attack of the nitrogen radical on the double bond [31], the resulting four-membered azetidine ring being a not unlikely intermediate. All reactions described being radical reactions, and being that there is no reason to confer a different reactivity to the allyl- and diallylamine allyl groups, it is highly unlikely that there is a selectivity in the radical additions, the most probable result being that of the formation of copolymers of allylamine and diallylamine.

2.4 The Effect of Oxygen

For both allylamine films and co-polymers oxygen is included in the films, a predictable evidence given the high concentrations of radicals generated during the deposition process. To assess the effect of oxygen on the properties of the films, depositions were also made after careful purging of the deposition solutions with argon before the CV. The results are reported in Figure 2.8, while calculated charge transfer resistance values and other relevant electrochemical parameters can be found in Table 2.2. For both allylamine and 1:10 allylamine:diallylamine co-polymer films the charge transfer resistance is pushed to values above $70M\Omega$.
Significant changes are also present in the low frequency region of the

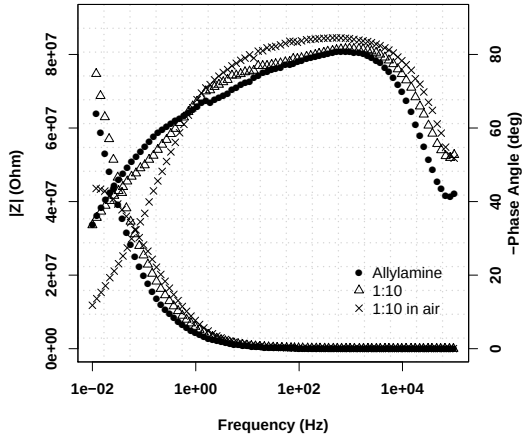

Figure 2.8: Impedance spectra of films deposited from a 10mM allylamine (•) and a 1:10 allylamine-diallylamine (Δ) solution after deoxygenation of the reaction mixture with Argon; a plot of a film deposited in presence of air from a 1:10 allylamine-diallylamine solution is shown for comparison (×).

phase angle plot, where lower values of the phase angle are reached, indicating a reduced ion permeability [34]; the lowest values remain around $-80°$ due to the high surface roughness of the electrode, while the high frequency region remains relatively unaltered.
While it is not possible at this stage to provide a precise mechanism for the polymerization, it seems that the removal of oxygen from the reaction mixture is instrumental in allowing the cross-linking to happen without hindrance. The layers obtained under deaerated conditions also show a remarkable stability over time, with no significant changes in the charge transfer resistance after one hour of immersion in either acetonitrile or water, meaning that no swelling due to solvent adsorption takes place.

Acknowledgements

Marcel Ceccato
Department of Chemistry, Langelansgade 140, 8000 Aarhus, Denmark

XPS spectra and XPS analysis.

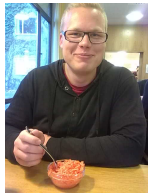

Jesper Vinther
Department of Chemistry, Langelansgade 140, 8000 Aarhus, Denmark

Scientific and non-strictly scientific support.

Mogens Hinge
Department of Engineering, Nymunkegade 120, 8000 Aarhus C, Denmark

Scientific support and helpful discussion and guidance.

Steen U. Pedersen
Interdisciplinary Nanoscience Center (iNANO), Gustav Wieds Vej 14, Aarhus University, 8000 Aarhus C, Denmark

Scientific support and helpful discussion and guidance.

Kim Daasbjerg
Interdisciplinary Nanoscience Center (iNANO), Gustav Wieds Vej 14, Aarhus University, 8000 Aarhus C, Denmark

Scientific support and helpful discussion and guidance.

Chapter 3

ORR Catalysis by Adenine Functionalized MWCNTs

Contents

The oxidative nature of oxygen, besides causing the premature failure of non-oxide materials, also makes it an ideal comburent. In particular, it is the *only* comburent which can be used by aerobic organisms including mammals, plants and many microorganisms, in order to produce energy by processing the fuels (a.k.a. food) previously converted to sugars or phophates. In the particular case of humans, playing such a central role in the functioning of metabolism also means that alterations in the consumption of oxygen can often be related to malfunctions of cellular activity. For this reason monitoring oxygen and its reduction products in cell cultures has been shown to be a way to discriminate between normal cells and cells affected by certain types of tumors[35]. On the other hand the exploitation of hydrogen as a fuel relies on the possibility to reduce oxygen efficiently in order to make the process energy efficient. In both instances, however, the overpotential needed for the reduction of oxygen[36] means that a catalyst is needed.
In terms of overpotential the best catalyst known for the reduction of oxygen is platinum, which, however, still has drawbacks: It is 1) rare and expensive and 2) prone to poisoning. While the first problem is often mitigated with mass production the latter is less easily avoided. In a biological environment in particular there is a wealth of molecules that can interfere with an electrochemical measurement

by adsorbing on the platinum electrode, especially at the relatively high potentials needed for the reduction of oxygen. From these considerations stems the interest for catalysts other than platinum.
Lately a considerable interest has been aimed at non-noble metals such as cobalt[37, 38, 39], as a relatively cheaper alternative to platinum, at all-organic catalysts[40, 41], and more or less elaborate combinations of the two[42, 43], with results on par or even better than those obtained with commercial platinum based catalysts[44]. In both cases catalytic performances only slightly less than those of platinum have been recorded which, together with the cheaper cost of the starting materials, make platinum-free systems competitive as a whole. The common problem with both cobalt complexes and organic molecules is their relatively short lifespan. If it is true that platinum is easily poisoned, it is also true that it can be regenerated. Organic and organo-metallic catalysts, while not as susceptible to poisoning, are more prone to degradation, with the additional obstacle that to be useful, they must be either anchored on a surface or separated from the reaction products. The immobilization step in particular can be tricky: it is often challenging to firmly anchor the catalysts on the surface, while at the same time achieving a high surface density and maintaining the catalyst active site accessible to the substrate.

3.1 Experimental Section

Electrochemical experiments were performed in an open cell with a platinum counter electrode and a saturated calomel reference electrode. In these conditions the oxygen concentration in solution is approximately 8mg/L[45]. Electrochemical experiments were performed with an AUTOLAB potentiostat and a Radiometer Analytical EDI rotating disk electrode equipped with Ø=3.5mm glassy carbon disk electrodes. The materials used to modify the working electrode are commercially available oxidized multi-walled carbon nanotubes, and adenine-functionalized carbon nanotubes, designed

and synthetized by the group of prof. A. Bianco[46]. The motivation behind the choice of adenine for the functionalization was two-fold: on one hand adenine has an amine pending group which could be used to coordinate catalytically active species as in the original article by Singh et al. [46], on the other hand it should also improve the solubility of the nanotubes.

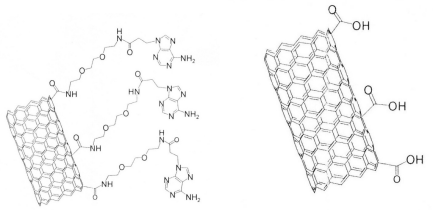

Figure 3.1: Left: structure of the adenine-functionalized multi-walled carbon nanotubes. Right: the commercially available oxidized carbon nanotubes

In Figure 3.1 a depiction of the two nanotube types is presented. From this point on, adenine functionalized CNTs will be referred to as *CNT-Ade*, while oxidized carbon nanotubes will be termed *CNT-COOH*. A thorough account of the functionalization steps can be found in an earlier work of prof. Bianco's group [46], however it should be noted that the synthetic procedure involves the use of strong acids. This should be emphasized, since one of the recurrent problems in the study of catalytic processes on carbon nanotubes, is that impurities in the form of metal nanoparticles, deriving from the CNT synthesis, are often present in the nanotube samples. These impurieties can possess catalytic activity themselves, making it at times difficult to unambiguously identify the true catalytic center[47, 48]. Acid treatments have been shown to effectively remove metal impurities from carbon nanotube samples[47]. It can be therefore stated that the results described in this work can be related with confidence to the carbon nanotubes alone.

3.1.1 Electrode Preparation

Glassy carbon disk electrodes 0.5cm in diameter were first polished with two alumina suspensions in water (grain sizes 0.5 and 0.003mm), then sonicated in doubly distilled water for 5 minutes. CNT-COOH and CNT-Ade suspensions were prepared by sonicating a small quantity of nanotubes in ca. 3ml of doubly distilled water for approximately 5 minutes.

For both CNT-COOH and CNT-Ade dispersions were prepared by

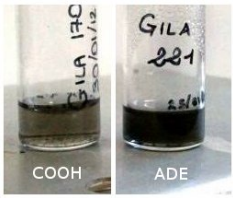

Figure 3.2: Dispersions of the oxidized (left) and adenine functionalized (right) carbon nanotubes.

adding a redundandant amount of material in the water, so that a precipitate was always present. In this way it was made sure that differences in the concentration of the dispersions would not be due to a different amount of starting material. As can be seen in Figure 3.2 the CNT-Ade dispersion is significanlty darker than the CNT-COOH one, without the need of any additive[49]. The drop-casting procedure involved the successive deposition of five 10μL drops; in between the depositions the solvent was allowed to evaporate with the aid of a mild heating. Electrodes were used immediately after preparation.

3.2 Catalytic Activity

The catalytic activity of the samples towards the reduction of oxygen was investigated by means of a *rotating disk electrode* (RDE): this electrochemical technique involves an electrode rotating around its axis, thereby generating a convective flux towards the electrode

surface, which effectively diminishes the diffusive contribution to the electrochemical current. This enables one to directly relate the measured current to the kinetics of the reaction under investigation by controlling the mass transport to the electrode through adjustments of the speed of rotation (see section 3.2.2 for details).
Experiments were conducted on three samples: CNT-COOH, CNT-Ade and a clean glassy carbon (GC) electrode, which acted as the non-catalytic reference material. The rotation speeds for all experiments were 0, 300, 1200, 2700 and 500rpm. Experiments were conducted at STP in an acqueous soluton exposed to air. In these conditions the concentration of dissolved oxygen is reported to be 8mg/L [45].

3.2.1 Experiments at Neutral pH

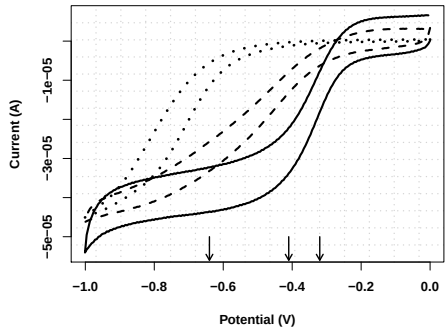

Figure 3.3: Cyclic voltammetries of a clean GC electrode (···), a CNT-COOH (- - -) and a CNT-Ade (—) electrodes at a speed of rotation of 1200rpm are shown. Experiments were carried out in 1x PBS with a saturated calomel reference electrode and a platinum counter electrode.

Experiments were at first carried out in a PBS 1x solution buffered at 7.4, in which the phosphate ions acted both as buffer and as supporting electrolyte. In Figure 3.3 the cyclic voltammetries for the GC, CNT-COOH and CNT-Ade samples at a speed of rotation of 1200rpm are shown. The arrows on the x-axis indicate the approximate half-wave potentials for the three curves. Both nanotube samples exhibit a clear anodic shift of the oxygen reduction, with CNT-Ade showing the lowest overpotential, roughlt 350mV lower than for the bare GC electrode, which compares very well with similar nanotube systems [41, 50]. Both for GC and CNT-COOH the current raises slowly and fails to reach a well defined plateau. For CNT-COOH this could be due to an imperfect film which could leave the GC substrate exposed and able to contribute to the reduction. This observation is backed by AFM images (Figure 3.4), which show mostly isolated nanotubes with large uncovered patches. The situa-

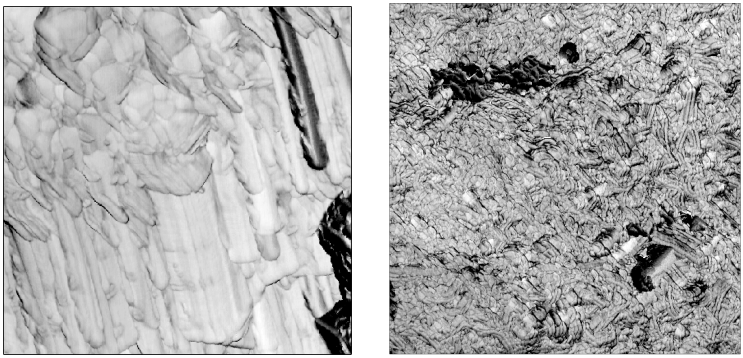

Figure 3.4: Left: AFM morphological image of a CNT-Ade deposit on ultraflat ITO; Bottom: AFM phase image of a CNT-COOH deposit on ultraflat ITO; in both cases the deposits were obtained by drop-casting 5 10μL drops of a dispersion of the nanotubes in doubly distilled water.

tion is different for CNT-Ade: micro-meter sized groups of nanotubes are clearly visible. These groupings also seem to have a well defined

orientation, making them more similar to well definied supramolecular assemblies. Being the only difference between CNT-COOH and CNT-Ade, adenine must surely be the source of the anisotropy, although at this stage the nature of the interaction which causes the effect is not entirely clear. It is plausible that either hydrogen bonding or $\pi - \pi$ stacking between the adenine groups on different carbon nanotubes can induce the alignment. An analysis of the literature in heterogeneous catalysis suggests that a likely cause of the better catalytic properties by the structuring is the formation of more kinks and edges, rather than a change in the kinetics of the process. It is generally accepted that defects on a surface are invariably more reactive than a plain, especially when adsorption is involved: a situation such as that depicted in Figure 3.5 might be responsible for the osberved differences between CNT-Ade and CNT-COOH. Aligned

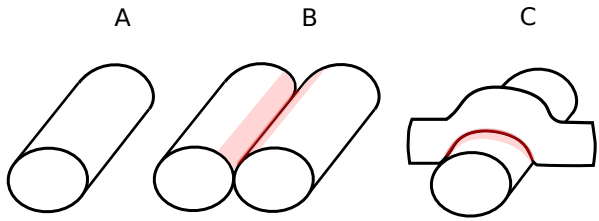

Figure 3.5: Sketch of possible nanotube alignments with the defect area where the catalysis of oxygen reduction might take place highlighted in red: A: isolated nanotube; B: aligned nanotubes; C: randomly dispersed nanotubes. If the source of the catalytic activity was correct, aligned nanotubes would create a larger area of active sites.

nanotubes would create kinks proportional to the nanotube lenght (Figure 3.5B) while randomly positioned nanotubes would generate a much lower surface area of defects (Figure 3.5C). This aspect of carbon nanotube activity towards oxygen reduction seems to have been overlooked in the vast literature on the topic. It would be of

interest to re-examine some of the results obtained so far with other CNT-based catalysts to better assess the true role of the surface functionalization.

Mass Effect on the Properties of CNT-COOH

As seen in Figure 3.2 CNT-Ade forms much darker, that is concentrated, dispersions than CNT-COOH. This increase is, in itself, a considerable advantage, likely caused by the interplay between the hydrophilicity of the adenine moiety, and the consequent lower tendency of the nanotubes to form disordered aggregates which prevent them from leaving the solid phase. This is also evident from the AFM images of FIgure 3.4, where it was shown that the adenine surface groups induce a surface structuring of the nanotubes.

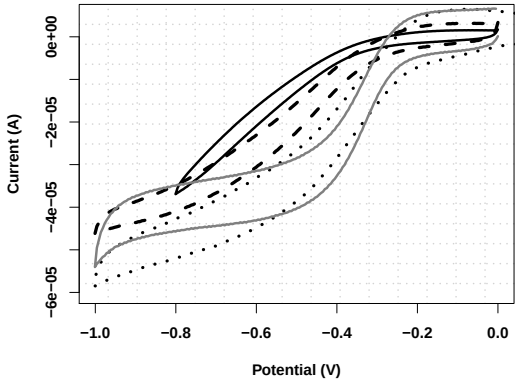

Figure 3.6: Voltammograms obtained after deposition of 3 (—), 5 (- - -) and 10 ($\cdots$) 20μL drops of a CNT-COOH dispersion; the voltammogram showing a 5 drop drop-cast of CNT-Ade (—) is also shown for comparison

To understand whether the higher catalytic activity is to be ascribed to the higher surface coverage, to the higher surface order, to variations in the reaction mechanism or to a combination of the above, experiments were also performed at higher surface coverage of CNT-COOH. Three electrodes on which the drop-cast of CNT-COOH was performed with 3, 5 and 10 10μm drops of the same dispersion were prepared to obtain a higher surface coverage of CNT-COOH and thereby gauge its effect on the catalytic properties of the deposits. The results reported in Figure 3.6 show how a noticeable anodic shift is observed as the surface concentration of CNT-COOH grows, until a reduction potential close to that of CNT-Ade is reached. Drop-casting more than 10 drops of CNT-COOH did not bring about further changes in the ORR reduction potential. Despite the similar half-wave potential the steady state region (¡-0.45V) remains much more well defined for CNT-Ade, meaning that regardless of the quantity of deposited material, CNT-Ade is able to give a more homogeneous covering of the electrode surface thanks to the auto-structuring of the functionalized nanotubes.
This result confirms that surface coverage has a strong influence on the observed catalytic properties, which leads one to think that the reaction mechanism does not change between CNT-COOH and CNT-Ade; this point will be explored in the next section.

3.2.2 Kinetic Analysis

An analysis following the theory developed by Koutechy and Levich was performed in order to calculate the number of electrons exchanged in the rate determining step of the reduction of oxygen, and the heterogeneous rate constant. The treatment is based on the equation

$$\frac{1}{J} = \frac{1}{J_K} + \frac{1}{J_L} = \frac{1}{J_K} + \frac{1}{B(\omega)^{\frac{1}{2}}} \tag{3.1}$$

where J is the total current density and J_K and J_L are defined as follows

$$J_K = nFk_{ET}C_0 \tag{3.2}$$

$$\frac{1}{B} = \frac{1}{0.62nFC_0D^{\frac{2}{3}}\nu^{-\frac{1}{6}}} \tag{3.3}$$

that is as the kinetic and the convective terms respectively. A fit of the inverse of the current density vs the inverse of the square of the speed of rotation of the electrode for various speeds of rotation produces a straight line, from the fitting of which the parameters n and k_{ET} can be extrapolated. In Figure 3.7 both the results of the

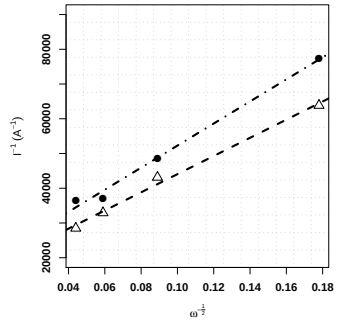

	n	$\mathbf{k}_{ET}$
Δ	1.9	$1.5 \cdot 10^{-2}$
$\bullet$	1.6	$1.5 \cdot 10^{-2}$

Figure 3.7: Values of the number of electrons transferred in the rate determining step (n) and of the heterogeneous rate constant (k_{ET}) as obtained from a Koutechy-Levich analysis of the voltammetries recorder at pH=7.4. In the Koutechy-Levich plot both data relative to CNT-Ade ($\bullet$) and CNT-COOH (Δ) are shown.

fitting and the resulting values for n (number of electrons exchanged in the rate determining step) and k_{ET} (heterogeneous rate constant) are given. The data show that the kinetic parameters are invaried between CNT-COOH and CNT-Ade: for both materials the reduction is found a 2-electron process and no difference in the speed of

the process were recorded. The enhancing effect of nitrogen groups on the catalytic properties of carbon materials towards the ORR has already been observed[50], altough no clear explanation of the phenomenon has yet been put forward. In the present case the evidence accumulated seems to support the possibility that the increase in catalytic activity is not due to changes in the reaction mechanism or in the electronic structure of the catalyst, but to favorable changes in the surface morphology. An example of such a relationship can be found in a particularly insightful work by Matsubara et al.[51], in which it is demonstrated how the presence of pentagonal defects and rounded compartments on the surface of MWCNTs enhances their ORR activity. A comparison with the bare glassy carbon was also attempted in order to exclude any substrate effects. As evidenced in the cyclic voltammeries, however, the Koutechy-Levich model could not be applied profitably due to the particular current response on glassy carbon. This is reasonably due to two concomitant factors: on one hand the cathodic potential at which oxygen reduction occurs on GC is close to the water reduction potential, which likely contributes to the total current registered, on the other hand it cannot be ruled out that the reduction reaction is not stricly first order, as is required by the Koutechy-Levich formalism.

3.2.3 Experiments at Acid pH

In practical applications variations in pH are often encountered, especially when considering redox reactions such as the reduction of oxygen, which involve hydronium ions. This is particularly true in the vicinity of cells, which, as a consequence of their metabolism, expell various chemicals which affect the concentration of hydronium ions (ROS, RNS, ...). The reduction of oxygen is notoriously influenced by pH variations, as is the response of catalysts[49]. In order to gain an appreciation of the response of the nanotubes to pH changes RDE experiments were conducted in citrate buffers at pH 4 and pH 6. This also allowed the examination of their behavior with a chemical compound, the citrate ion, which is known to adsorb on

platinum [52], the material most commonly used for oxygen sensing. From Figure 3.8 it is apparent how CNT-Ade is the only sample which does not suffer a variation of catalytic activity at acid pH; a pH of 6 is sufficient to significantly alter the shape of the voltammograms for GC and CNT-COOH. In both instances the peak current diminishes and there is an shift of the reduction potential towards more cathodic values, with the disappearance of a steady state.

At pH 4 in the case of glassy carbon, an inversion is seen between

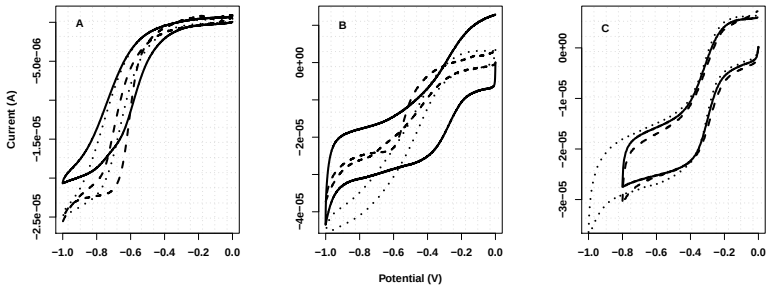

Figure 3.8: Effect of varying pH on the catalytic properties of the samples A: glassy carbon; B: CNT-COOH; C: CNT-Ade. Experiments were conducted in 1x PBS buffer at pH 7.4 (· · ·), and in a citrate buffer at pH 6 (—) and at pH 4 (- - -).

the forward and back scans, the current being higher in latter. This effect suggests that the reactive radicals generated in the reduction of oxygen attack the surface and are desorbed only at a later stage, when the potential is inverted. A similar behavior is observed with CNT-COOH, albeit only at potentials approximately 100mV past the beginning of the steady state. At the same time, the voltammetries of CNT-Ade are remarkably insensitive to the increasingly acid environment. It should be noted that the best results for CNT-COOH were obtained at pH 4. This fact suggests that the highest catalytic response on the nanotubes is achieved when surface groups

are protonated. It is then to be expected that by choosing a sufficiently basic pH, one could deprotonate the basic nitrogen on adenine and similarly degrade its catalytic properties. This implies that one can change the pH window in which the CNTs are active as catalysts by tailoring the pKa of their surface groups by functionalization with an appropriate molecule.

3.3 Conclusions

A new variant of multi-walled adenine functionalized carbon nanotubes developed by the group of prof. A. Bianco was studied in relation to the reduction of oxygen in water. Both commercial oxidized MWCNTs (CNT-COOH) and the adenine functionalized MWCNTs (CNT-Ade) are able to catalyze the reduction of oxygen as demonstrated by the comparison with glassy carbon, a non-catalytic material. CNT-Ade shows a higher solubility and the ability to assemble into ordered structures on the electrode surface in the form of aligned assemblies of nanotubes, which causes an anodic shift of the reduction potential larger by 100mV with respect to CNT-COOH. Depositing a larger quantity of CNT-COOH on the electrode surface helps bring the reduction potential of oxygen close to that measured on CNT-Ade, but the latter still shows a more well defined steady state, indicative of a better surface coverage. A kinetic analysis has not revealed significant differences in the number of electrons exchanged nor in the heterogeneous kinetic constant between CNT-COOH and CNT-Ade, indicating that the different catalytic behavior is entirely due to surface structuring effects which, in the case of CNT-Ade, likely lead to a higher surface area of the kinks at which the reduction reaction might take place. In view of a possible application in the sensing of oxygen in biological environments, experiments at acid pH were conducted: these show how covering the nanotubes with adenine allows to retain their catalytic properties even at pH 4, while surface protonation of the acid groups present on the surface of CNT-COOH leads to a loss of catalytic activity at

pH less than 7. Overall, adenine functionalization has proven to be a very effective way to achieve better solubility in water, surface order which leads to improved catalytic performance and stability at acid pH.

Acknowledgements

Elena Villani
G. Ciamician Chemistry Department, via Selmi 2, 40126 Bologna, Italy

Graduate slave labor and scientific as well as non scientific support.

Alberto Bianco
NRS UPR 9021, Institute Of Molecular And Cellular Biology, 67084 Strasbourg, France

Head of the group which developed the idea and synthesis of CNT-Ade and provided the materials analyzed.

Chapter 4

Catalysis of water oxidation by hydrogel dispersed polyoxometallates

Contents

Since their discovery carbon nanotubes have seen a constant rise in popularity. This is both due to their unique mechanical and chemical properties, and the possibility to exploit their high surface area to chemically modify them before depositing them on a surface, thus reaching extremely high surface densities of the molecule of interest. Lately, also supramoleular assemblies of carbon nanotubes with catalytic species such as polyoxometallates (POM) have been reported, in which synergyc effects enhance the catalytic activity of the oxygen evolving POM. One of the chief problems related to the employment of CNTs is their scarce solubility both in organic solvents and, most notably, water, caused both by their usually large size and by their extremely hydrophobic character. While numerous successful attempts have been made at chemically modifying carbon nanotubes in order to enhance their hydrophilicity; in this work we have focused our attention on the study of two new possible solvents, developed by Dr. A. Di Crescenzo in the group of prof. A. Fontana at the University of Chieti. These molecules form hydrogels that allow the formation of stable and concentrated dispersions of pristine CNTs without the need of any surface functionalization, the strategy most often employed to make the CNTs water soluble. This result opened

up the possibility to subsequently disperse a recently developed oxygen evolving species, in the form of a supramolecular complex made up of single wall carbon nanotubes and polyoxometallates with a Ruthenium metallic core; the polyoxometallates were provided by the group of M. Bonchio at the university of Padua, and have been shown to be oxygen evolving centers[53, 54].

4.1 Experimental Section

The two tensioactive molecolecules developed by the group of Dr. A. Di Crescenzo are p-dodecyloxibenzyl-dimethyl-amine oxide (pDOAO) and p-dodecyloxibenzyl-trimethyl-amine bromide (pDOTABr), a zwitterion and a bromide salt respectively. The polyoxometalate was synthetized by the group of M. Bonchio and features a decatungstosilicate ligand in which a tetraruthenium(IV) core is embedded[55]. Electrochemical experiments were performed with a BIOLOGIC potentiostat and DROPSENS DRP-110 screen printed electrodes, featuring glassy carbon working (Ø=5mm) and counter electrodes and a silver reference electrode. The hydrogels were deposited on the electrodes using a micropipette. Enough material was deposited in order to completely cover all the electrodes on the DROPSENS subtrate.

4.1.1 Hydrogel preparation

All gels were prepared using distilled water as the solvent and commercially available purified single-wall carbon nanotubes. **pDOAO** and **pDOTABr** gels were prepared from 100mM solutions of the respective molecules. For **pDOTABr** 100mM NaBr was also added in order to favor gelification. The solutions were then stirred for 30 minutes at STP until a gel formed.
pDOAO hydrogels containing single-walled carbon nanotubes, were prepared by first sonicating the nanotubes in a 5mM pDOAO solution for 4 hours. pDOAO was then added to the solution in order to reach a concentration of 100mM. The solution was then stirred for

30 minutes until the gelification occurred.
pDOTABr/SWCNT hydrogels were prepared by sonicating the nanotubes in a 2mM pDOTABr solution for 4 hours. The concentration of pDOATBr was then brought to 100mM and 100mM NaBr was added. The mixture was then stirred for 30 minutes.
pDOATBr/SWCNT/POM hydrogels were prepared by first sonicating SWCNTs with 1mM pDOATBr for 4 hours. A 10mM POM solution was prepared separately. The two solutions were then mixed and stirred for 1 hour. The concentration of pDOATBr was then raised to 100mM and 100mM NaBr was added. The resulting solution was then stirred for 30 minutes.

4.2 Electrochemical Characterization

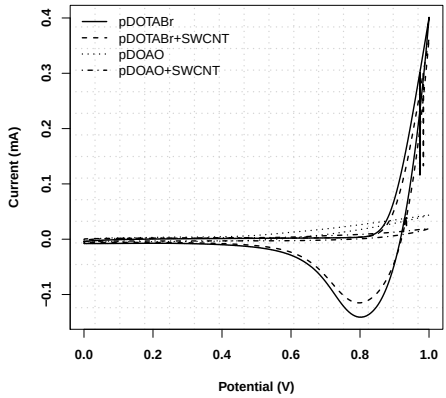

Figure 4.1: Cyclic voltammetries of the gels pDOTABr with (- - -) and without (—) single walled carbon nanotubes, and pDOAO with (···) and without (· – · –) single walled carbon nanotubes.

The electrical properties of the gels were investigated by means of cyclic voltammetry and electrochemical impedance spectroscopy. Figure 1 shows the anodic scan for pDOTABr and PDOAO. The reponse of pDOTABr is similar to that of an electrolytic solution, with a low capacitive current and resistance. pDOAO on the other hand shows weaker signs of redox activity. A likely cause of this result could be the low self diffusion coefficient for pDOAO, given its zwitterionic nature. This characteristic would make the charge compensation needed for an electrochemical process to happen rather difficult, thereby slowing down the electrochemical reaction and demanding higher overpotentials for it to occur. This supposition however is not backed experiments, as will be discussed in the next subsection.

4.2.1 pDOAO

In order to try and compensate the absence of separate ionic pairs smaller, more mobile ions in the form of lithium chloride were added to pDOAO. As can be seen from the results of the fitting of the impedance spectra presented in Table 4.1, however, the addition only has the effect of diminishing the gel resistance from 500 to 70 Ohms without significantly affecting the outcome of the voltammetric measurements. The cyclic voltammetries remain, in fact, relatively unaltered across the samples with increasing LiCl concentration (Figure 4.2.) These results are rather puzzling, in that while the solution resistance seems to be low enough to allow redox reactions to happen unhindered, the overpotential for water oxidation seems to tell a different story. Impedance measurements run on pDOAO and pDOTABr confirm that the gel resistance does not vary significantly between the two gels, being in the order of a few hundred Ohm in both cases. The charge transfer resistance, on the other hand, changes significantly between pDOAO and pDOTABr, regardless of the presence of nanotubes. While a Randle's circuit modified with a constant phase element (CPE) was used in all cases for pDOAO, the addition of a charge transfer resistance to fit the spectra of pDOTABr invariably caused a doubling of χ^2. The best fit was obtained by

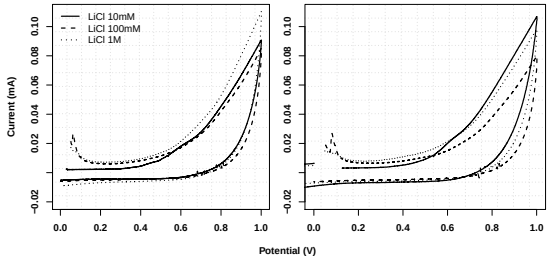

Figure 4.2: Left: cyclic voltammetries in gel pDOAO. Right: cyclic voltammetries of gel pDOAO with SWCNTs. In each pane the voltammetries of gel pDOAO with 10mM (—), 100mM (- - -) and 1M ($\cdots$) lithium chloride are presented.

using a resistance and a (CPE) in series, indicating a small if not absent charge transfer resistance. The source of the different behavior of the two gels is not fully understood, although the experimental data available seems to point to a film-like blocking of the surface by pDOAO. Whether this blocking occurs via the formation of a film of pDOAO on the surface, or whether it is caused by a very low self diffusion coefficient of pDOAO which brings about a film-like passivation is, however, unclear. Scanning electron microscopy images of the lyophilized gel (Figure 4.3, courtesy of A. Di Crescenzo and A. Fontana) show the formation of lamellar structures in solidified pDOAO, which might validate the hypothesys of the formation of a film. When put in contact with a an electrode the lamellae could, in fact, orientate themselves parallel to the charged surface and act as a passivating film. More work and possibly theoretical insight is needed to better comprehend this matter, including the orientation of pDOAO molecules inside the lamellae, as it might also be of interest to better comprehend the behavior of ionic liquids at interfaces. As for the current project, in view of these results the catalytic properties of POM were only tested in pDOTABr, since the physico-

Table 4.1: pDOTABr with SWCNTs (pdotaBR), pDOAO with SWCTNs (pdoaoS), and pDOAO with 10mM (pdoaoA), 100mM (pdoaoB) and 1M (pdoaoC) LiCL

	R1	Q2 ($\cdot 10^{-6}$ Fs^{a-1})	a	R2
pdoaoS	352.1	13.49	0.90	1.94e6
pdoaoA	506.3	21.41	0.85	2.02e6
pdoaoB	230.9	15.69	0.91	1.72e6
pdoaoC	70.78	13.41	0.91	2.66e6
pdotaBR	91.44	25.86	0.90	/

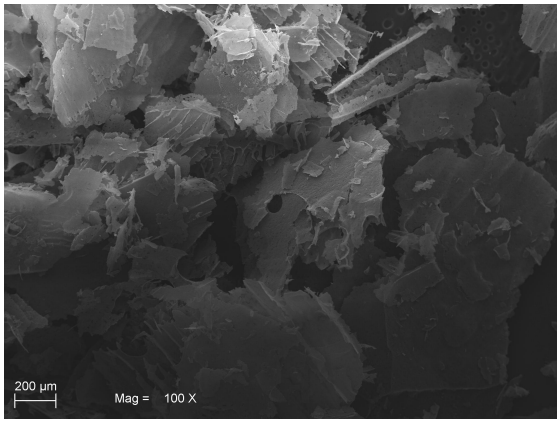

Figure 4.3: SEM micrograph of a lyophilized pDOAO sample.

chemical properties of pDOAO make it unsuitable for the purpose of electrochemical reactions.

4.3 Catalysis in pDOTABr

Cyclic voltammetric experiments were performed in order to gauge the catalytic activity of the POM inside the gel PDOTABr. Three samples were compared at first: the pDOTABr gel (gNO), pDOTABr gel with SWCNTs (gCNT), pDOTABr gel with SWCNTs and POM (gSPOM). As is shown in Figure 4.4 the voltammetries are flat with up to 0.87V for gNO and gCNT, where the oxidation of water begins[53]. gSPOM has a 100mV cathodic shift with respect to the samples without POMs, while little discernible variations are encountered between gNO and the sample containing only carbon nanotubes gCNT. This implies that the catalytic activity is solely due

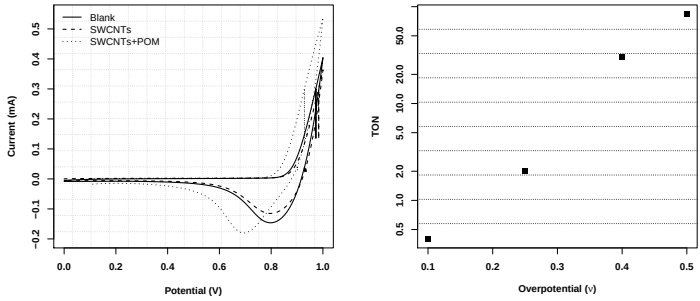

Figure 4.4: Left: Cyclic voltammetries of sample gSPOM (· · ·) at pH 7 showing the onset of water oxidation. The curves pertaining to sample gCNTs (- - -) and the gel pDOTABr (—) are also shown for comparison. Right: calculated Turn Over Number (TON) values for sample gSPOM at pH 7 (■).

to the polyoxometallates, the catalytic properties of which are not negatively affected by the hydrogel. On the right in Figure 4.4 the calculated turn over number values for gSPOM are shown. The values were obtained by running a chronoamperometric measurement, that is an experiment in which the current is continuously measured

as a square potential wave of progressively increasing magnitude is applied at 1 minute time intervals. From the integration of the measured current we were able to calculate the TON (Turn Over Number) at the different applied potentials. The TON is a commonly used measure to compare catalytic activity between molecular catalysts, that is defined as the maximum numer of molecules a catalyst can convert per unit site per unit time. In the electrochemical case these numbers can be derived from measured currents as follows:

$$\frac{Q_m - Q_b}{Q_{cat}} \tag{4.1}$$

where Q_m is the measured charge, Q_b is the charge baseline (arising from i.e. capacitive contributions and non relevant reactions) and Q_{cat} is the number of catalyst molecules calculated as the charge needed to oxidize/reduce all the catalyst on the electrode. In the present case, the latter quantity was obtained from the reduction of the polyoxometallates at pH4 (4.5), where it is most well defined. Calculation of TON values (Figure 4.4) shows that they are directly comparable to those previously reported for the surface absorbed CNT-POM complex in water[53], proving that the efficiency of the catalyst is not thwarted in the new environment.

4.3.1 Effect of pH

Being known that the oxidation of water and the catalytic activity of polyoxometallates are both pH dependent, experiments were also conducted in gels containing different concentrations of hydronium ions. Figure 4.5 shows the results of such experiments, in which the pH of gCNT and gSPOM was changed to 1, 4 and 8 by adding the appropriate amount of HCl NaOH to the distilled water during synthesis. gCNT does not show significant variations at different pH values, while gSPOM shows an increased catalytic activity as the acidity is lowered to pH 4, while at pH the voltammetry resembles that at neutral pH. The effect of pH has also been investigated in relation to the cyclic voltammetry of POM, where it can be seen

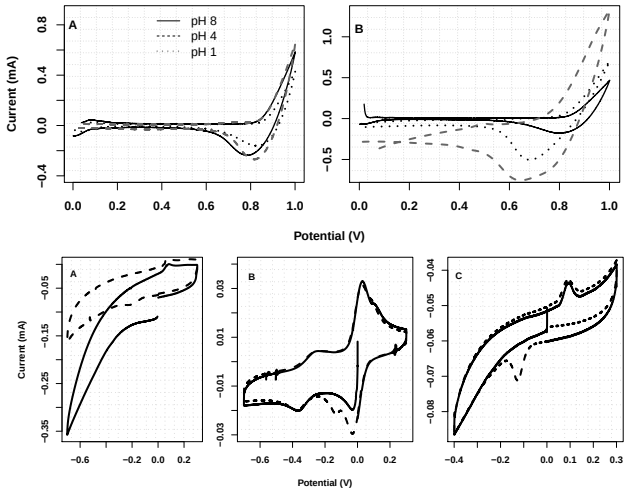

Figure 4.5: In the top half cyclic voltammetric experiments at different pH of sample A: gCNT, and B: gSPOM are presented. In both graphs the different line traits identify experiments performed at pH 8 (—), pH 4 (- - -) and pH 1 (· · ·). In the bottom half cyclic voltammetric experiments showing the reduction of POM at A: pH 8, B: pH 4 and C: pH 1 are presented.

that also the reductive behavior of the polyoxometalate is more well defined at pH 4. The voltammetric peaks have been previously identified as a result of the reduction of the polyoxometalate ligand[56]: the pH dependance can then be ascribed to the protonation of the surface OH groups, which, it has already been shown, contribute to the electrochemical behavior of the complex[57]. All these results suggest that the hydrogel is an excellent medium to disperse carbon nanotubes and polyoxometallates, and that the electrochemical behavior of the POM is not modified in the new medium.

4.3.2 Effect of Prolonged Oxidation

Tests were conducted to gauge the effect of the oxidation of water over time on the gel. After roughly 15 minutes of oxidation at a current density of 0.4mA/cm^2 small micrometer sized particles appeared, likely due to the precipitation of the tensioactive after excessive dehydration. The gel was then put in contact with distilled water in order to try and achieve a balance between the water oxidized and that adsorbed from solution; the choice of distilled water instead of a ionic solution is also justified by the sharper contrast in resistivity with the hydrogel as seen with impedance, which would make it easier to understand whether the gel is being brought into solution and the electrode surface is thus being exposed to the water. Impedance measurements were run at fixed time intervals to monitor the stability of the hydrogel. As is visible from the Z-modulus and particularly

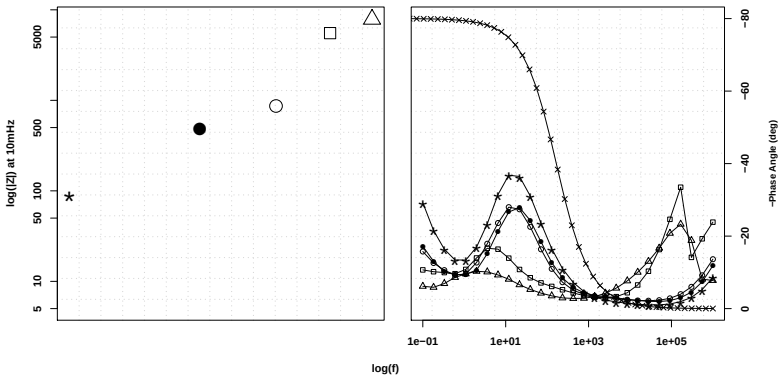

Figure 4.6: Maximum of the absolute value of the impedance (left) and phase angle plots (right) at different intervals after immersion of the electrode covered with the hydrogel in distilled water. The different symbols correspond to measurements before the immersion in water ($\times$, phase only), and after 10 minutes ($*$), 25 minutes ($\bullet$), 45 minutes ($\circ$), 60 minutes ($\square$) and 75 minutes (Δ) from immersion.

from the phase angle plot in Figure 4.6, there is evidence that instead of a slow re-hydration of the hydrogel, there is an infiltration of a water layer between the hydrogel and the electrode surface, as evidenced by the increasingly resistive behavior of the cell; this is apparent in the flattening of the phase angle towards values close to 0° and in the increase of the total impedance, due to the fact that, since it did not contain any electrolyte, the water in which the electrode was immersed was very resistive. This fact poses a challenging engineering problem which, as of now, hinders the transformation of the developed system to a working device; work is currently underway to assure the stability of the hydrogels even in acqueous enviroments. This drawback does not, however, diminish the general applicability of the hydrogel as a dispersing medium for nanotube-based catalysts: particularly in the case of gaseous analytes, it should be possible to taylor the thickness of the hydrogel layer on the electrode to the diffusion coefficient of the analyte through the hydrogel, thereby potentially achieving a sufficiently high efficiency.

4.4 Conclusions

The poperties of two hydrogels based on the tensioactives pDOAO and pDOTABr were studied. Both hydrogels are excellent dispersing mediums for highly insoluble carbon nanotubes. The fact that their constituents (water and a non toxic tensioactive) potentially make them chemically and environmentally harmless adds to their value as dispersing mediums. Their electrochemical properties show that only pDOTABr is suitable for electrochemical experiments, while pDOAO exhibits a high charge transfer resistance which might be linked to the formation of ordered planar assemblies of the pDOAO molecule, a characteristic which should be the object of further analysis. A single-wall carbon nanotube-polyoxometallate supramolecular complex was subsequently dispersed in pDOTABr to test the possibility to use it as a medium to solubilize nanotube based catalysts in water without the need of further functionalization with hydrophilic

groups. Electrochemical experiments show that the POM catalyst maintains its water oxidation activity in the new medium.

Acknowledgements

Antonello Di Crescenzo
Dipartimento di Scienze del Farmaco Università "G. d'Annunzio"
Via dei Vestini 31 66013 Chieti

Synthesis of the hydrogels and of the CNT-POM dispersions therein, and SEM analysis.

Antonella Fontana
Dipartimento di Scienze del Farmaco Università "G. d'Annunzio"
Via dei Vestini 31 66013 Chieti

Group leader. Synthesis of the hydrogels and of the CNT-POM dispersions therein.

Appendix A

Electrochemical Impedance Spectroscopy

Contents

Electrochemial impedance spectroscopy (EIS) is based on the measurement of a current in response to an applied potential perturbation in the form of a sine wave. The measured current is linearly proportional to the applied potential

$$V = Z \cdot i \tag{A.1}$$

which is Ohm's Law, with one fundamental difference: in place of a resistance R, a new proportionality constant is used, the impedance Z. The impedance is defined as the resistance plus the contribution of another quantity, the reactance X,

$$Z = R + i{\cdot}X \tag{A.2}$$

which describes the response of the system to variations in the applied potential, rather than to a steady potential. This difference is quite important. In an EIS experiment a potential varying as a sine wave is applied, and a current similarly varying as a sine wave is recorded. As is depicted in Figure A.1, however, the response of the system to a change in potential is not instantaneous; this causes the current to *lag* behind the potential. The cause behind this behavior is that every electrochemical cell has a capacitive contribution, and the charging of the capacitor is not an instantaneous process.

A.1 The Double Layer

The presence of a capacitor in the electrochemical cell follows from the formation of a double layer, a process which happens at the sur-

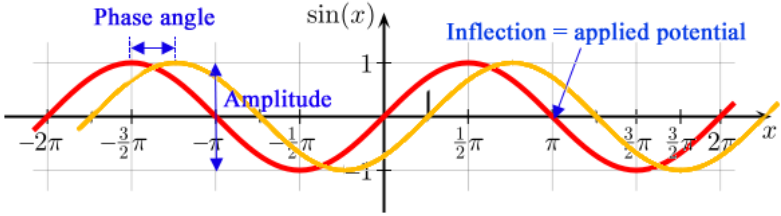

Figure A.1: Representation of a sinusoidally varying potential (red) and the resulting sinusoidally varying current (orange) with the lag (phase angle) between the two.

face of any conductive material placed in an electrolytic solution. Any surface bears a certain amount of charge, even more so if this charge is willfully generated by the application of a potential. The ions in solution will react to the electric field created by the surface charge of the material according to the laws of electrostatic interaction, that is like charges repell eachother, unlike charges attract eachother. This will lead to a structuring of a layer of solution in

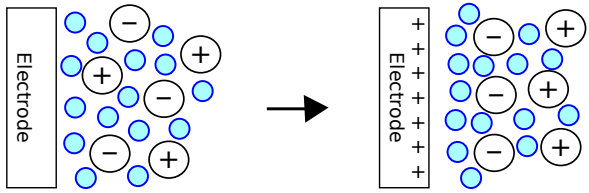

Figure A.2: Depiction of the structuring of an electrolytic solution, also known as formation of a double layer, in response to the charging of an electrode. Solvent molecules are represented in blue.

contact with the surface, forming what is termed the *double layer* (Figure A.2).

An analogy can be made between the double layer and a capacitor: there are two plates of opposite charges (the surface/electrode and the ions in solution) separated by a dielectric material (solvent molecules or a film on the surface). In this way the physical treatment of capacitors as seen in electrical circuits can be transferred to the electrochemical case

$$C = \frac{\epsilon \cdot \epsilon_0 \cdot A}{d} \tag{A.3}$$

where A and d are the area of the electrode and the distance between the surface and the layer of ions respectively, while ϵ and ϵ_0 are the permittivity of the medium which separates the two plates and that of vacuum respectively. The impedance of a capacitor is defined as

$$Z = \frac{1}{i\omega C} \tag{A.4}$$

with i=$\sqrt{-1}$, C the capacitance as defined in Equation A.3 and ω the angular frequency at which the potential is varied.
Since one half of the double layer is made up by ions in solution, and these are able to drift through the solvent at a speed determined by their diffusion coefficient in that particular solvent, it can be foreseen how the building of the double layer will require a certain time, as any adjustment to its structure due to a change in the applied potential. This is the origin of the time dependance which requires the use of the impedance in place of a resistance Equation A.1.

A.1.1 The Constant Phase Element

It can happen that a capacitor is inadeguate to describe certain electrodes. This is due to the electrode surface not being a perfectly flat slate, but having various kinds of inhomogeneities. These inhomogeneities make the capacitance vary across a surface according to the surphace morphology. The practical solution to this problem is the use of a constant phase element (CPE)

$$Z = \frac{Q}{(i\omega)^n} \tag{A.5}$$

A comparison with Equation A.4 reveals that the capacitance C has been substituted with Q, the impedance at ω=1rad/s, while the term iω is now weighted by an exponential n, with $0 \leq n \leq 1$.
A quick analysis shows that at n=1 the impendace is that of an ideal capacitor, while $n = 0 \Rightarrow Z = Q \Rightarrow Z \neq Z(\omega)$, that is the impedance is that of an ideal resistance.

A.1.2 The Resistance

Similarly, other electronic components are used to describe electrochemical cells i.e. resistances are used to represent electrochemical reactions or diffusion of molecules. The discharge of the double layer/capacitor can happen both if the application of the potential is discontinued, and if charge is allowed to *leak* away from the surface and to the solution via an electrochemical reaction. The most common situation is that in which one of these alternative pathways is present, in which case the electrode is modelled with a capacitor and a resistance connected in parallel (Figure A.3). A variation of the

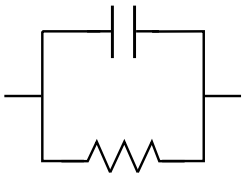

Figure A.3: A resistance and capacitor connected in parallel, one of the most often encountered building blocks in the modelling of EIS.

circuit shown in Figure A.3 that features another resistance preceding the elements in parallel is one of the most often encountered in electrochemistry and i termed the Randles circuit after its creator. The added resistance is used to account for the solution resistance.

A.2 Frequency and the Phase Angle

Since ions have a mass, the frequency at which the potential is varied will also heavily influence the response of the electrode, since more or less time will be allowed for the adjustment of the double layer. Moreover, if the motion of the ions is hindered (i.e. by a porous film) the frequency at which the blocking effect will be visible will also be informative as to the nature of the species and the process involved. This is particularly true when examining the *phase angle*, that is the time lag between the application of the potential and the current response as depicted in Figure A.1.

Phase Angle of Ideal Components

An ideal resistance, being frequency independent, will not show any phase angle. That is, the current response to the potential will be near instantaneous. In a phase angle plot this means having a phase angle equal to 0.

An ideal capacitor on the other hand will show a phase angle equal to -90°, where the negative sign is very important to distinguish it from another rarer circuit element, the inductance (phase angle=+90°), which will not be discussed here.

A constant phase element will show a phase angle slightly higher than an ideal capacitor: a value of -80° is, in fact, indicative of CPE behavior.

The phase angle is then a clear indicator of the capacitive or resistive nature of the impedance, and the frequency at which the behavior occurs tells something about the speed at which the process happens. The height of the capacitive loop can reveal information about the nature of the surface species which cause capacitive behavior: roughly speaking a uniform, compact film will show a phase angle in the range -70/-90°, while a less homogeneous/stable coverage such as that encountered in an adsorption/desorption process might cause

more depressed phase angle peaks at values $\leq 50°$. Moreover, low frequency loops might reveal adsorption/desorption or hindered (a.k.a slower) diffusion of bulkier ions, while high frequency loops are usually related to double layer reorganization or solvent motion, that is the higher the frequency, the more mobile/smaller the species which is able to respond to the potential variations is. Impedance is usually measured up to 1MHz; it might be revealing that TeraHertz spectroscopy is a powerful tool to investigate solvent structure by directly probing the collective motion of domains of solvent molecules.

Bibliography

[1] Akira Wada, Yasutaka Honda, Syuhei Yamaguchi, Shigenori Nagatomo, Telzo Kitagawa, Koichiro Jitsukawa, and Hideki Masuda. Steric and hydrogen-bonding effects on the stability of copper complexes with small molecules. *Inorg. Chem.*, 43:5725–5735, 2004.

[2] N. K. Patel and J. Franco. Amines as corrosion inhibitors for copper. *Materials and Corrosion*, 26(2):124–125, 1975.

[3] E Stupnishek-Lisac, A Brnada, and A.D Mance. Secondary amines as copper corrosion inhibitors in acid media. *Corrosion Science*, 42(2):243 – 257, 2000.

[4] M. Scendo. The influence of adenine on corrosion of copper in chloride solutions. *Corrosion Science*, 50(7):2070 – 2077, 2008.

[5] The Hendrix Group Inc. Notes for copper alloy corrosive table. Accessed 2013-03-01.

[6] Peizhen Shi, Qiming Wang, Yimin Xu, and Wei Luo. Corrosion behavior of bulk nanocrystalline copper in ammonia solution. *Materials Letters*, 65(5):857 – 859, 2011.

[7] Anodamine Inc. Copper corrosion and protection. Accessed 2013-03-01.

[8] Ho Yeung H. Chan, Christos Takoudis, and Michael J. Weaver. Oxide film formation and oxygen adsorption on copper in acqueous media as probed by surface-enhanced raman spectroscopy. *J. Phys. Chem. B*, 103:357–365, 1998.

[9] A. Migdal-Mikuli, E. Mikuli, M. Baranska, and L. Hetmanczyk. vibractional spectrum and molecular structure of $[cu(nh_3)_5](clo_4)_2$. *Chem. Phys. Lett.*, 381:329–334, 2003.

[10] Xiaohui Zhang, Simo O. Pehkonen, Nikolai Kocherginsky, and Grant Andrew Ellis. Copper corrosion in mildly alkaline water with the disinfectant monochloramine. *Corr. Sci.*, 44:2507–2528, 2002.

[11] Y. Feng, W.-K. Teo, K.-S. Siow, K.-L. Tan, and A.-K. Hsieh. The corrosion behavior of copper in neutral tap water. part i: corrosion mechanisms. *Corr. Sci.*, 38:369–385, 1996.

[12] J. F. Rios, J. A. Calderon, and R.P. Nogueira. Electrochemical behavior of copper in drinking water: evaluation of dissolution process at low anodic overpotential. *J. Braz. Chem. Soc.*, 22:1362–1370, 2011.

[13] Alireza Mohadesi, Ashraf Salmanipour, Sayed Ziae Mohammadi, Ali Pourhatami, and Mohammad Ali Taher. Stripping voltammetric determination of copper (II) on an overoxidized polypyrrole functionalized with Nitroso-R. *Journal of the Brazilian Chemical Society*, 19:956 – 962, 00 2008.

[14] Kazuharu Sugawara, Shunitz Tanaka, and Mitsuhiko Taga. Accumulation voltammetry of copper(ii) at carbon-paste electrode containing salicylideneamino-2-thiophenol. *Fresenius' Journal of Analytical Chemistry*, 342:65–69, 1992.

[15] V. S. Ijeri and A. K. Srivastava. Voltammetric determination of copper at chemically modified electrodes based on crown ethers. *Fresenius' Journal of Analytical Chemistry*, 367:373–377, 2000.

[16] I. Toledo, M. Arancibia, C. Andrade, and I. Crivelli. Redox chemistry of copper acetate binuclear complexes in acetic acid-methanol mixture as solvent. *Polyhedron*, 17(1):173 – 178, 1998.

[17] Dianlu Jiang, Lijie Men, Jianxiu Wang, Yi Zhang, Sara Chickenyen, Yinsheng Wang, and Feimeng Zhou. Redox reactions of copper complexes formed with different beta-amyloid peptides and their neuropathalogical relevance†. *Biochemistry*, 46(32):9270–9282, 2007. PMID: 17636872.

[18] D. M. Bastidas, M. Criado, S. Fajardo, V. M. La Iglesia, E. Cano, and J. M. Bastidas. Copper deterioration: causes, diagnosis and risk minimization. *International Materials Reviews*, 55:99–127, 2010.

[19] Susumu Harada and Kiyoshi Shimizu. Process for producing polymers of monoallylamine, September 1985.

[20] Laurent Denis, Damien Cossement, Thomas Godfroid, Fabian Renaux, Carla Bittencourt, Rony Snyders, and Michel Hecq. Synthesis of allylamine plasma polymer films: correlation between plasma diagnostics and film characteristics. *Plasma Process. Polym.*, 6:199–208, 2009.

[21] Ji Zheng, Yoshihiro Ito, and Yukio Imanishi. Cell growth on immobilized cell growth factor. *Biomaterials*, 15:963–968, 1994.

[22] Ung-Jin Kim and Shigenori Kuga. Ion-exchange separation of proteins by polyallylamine-grafted cellulose gel. *J. Cromatogr. A*, 955:191–196, 2002.

[23] J. Bisquert, G. Garcia-Belmonte, P. Bueno, E. Longo, and L.O.S. Bulhoes. Impedance of constant phase element (cpe)-blocked diffusion in film electrodes. *J. Electroanal. Chem.*, 452:229–254, 1998.

[24] Minqi Zhao, Yuefen Zhou, Merlin L. Bruening, David E. Bergbreiter, and Richard M. Crooks. Inhibition of electrochemical

reactions at gold surfaces by grafted, highly fluorinated, hyperbranched polymer films. *Langmuir*, 13:1388–1391, 1997.

[25] Jeremy J. Harris and Merlin L. Bruening. Electrochemical and in situ ellipsometric investigation of the permeability and stability of layered polyelectrolyte films. *Langmuir*, 16:2006–2013, 2000.

[26] Marcel Ceccato, Lasse Tholstrup Nielsen, Joseph Iruthayaraj, Mogens Hinge, Steen Uttrup Pedersen, and Kim Daasbjerg. Nitrophenyl groups in diazonium-generated multilayered films: Which are electrochemically responsive? *Langmuir*, 26:10812–10821, 2010.

[27] Lasse Tholstrup Nielsen, Marcel Ceccato, Allan Hjarbæk Holm, Martin Verner Kristensen, Steen Uttrup Pedersen, and Kim Daasbjerg. Versatile transformations of alkylamine-derivatized glassy carbon electrodes using aryl isocyanates. *Langmuir*, 25:12160–12168, 2009.

[28] E. Punzón-Quijorna, V. Sánchez-Vaquero, A. Munoz Noval, D. Gallach Pérez, A. Climent Font, G. Ceccone, R. Gago, J.P. García Ruiz, and M. Manso Silván. Optimized allylamine deposition for improved pluripotential culture. *Vacuum*, 85:1071–1075, 2011.

[29] Andrei Choukourov, Hynek Biederman, Danka Slavinska, Luke Hanley, Andrey Grinevich, Hanna Boldyryeva, and Anna Mackova. Mechanistic studies of plasma polymerization of allylamine. *J. Phys. Chem. B*, 109:23086–23095, 2005.

[30] Randall Deinhammer, Mankit Ho, James Anderegg, and Marc Porter. Electrochemical oxdidation of amine-containing compounds: a route to the surface modification of glassy carbon electrodes. *Langmuir*, 10:1306–1318, 1994.

[31] Brian Wagner, Geraldine Ruel, and Janusz Lusztyk. Absolute kinetics of aminium radical reactions with olefins in acetonitrile solutions. *J. Am. Chem. Soc.*, 118:13–19, 1996.

[32] Hans Fischer and Leo Radom. Factors controlling the addition of carbon-centered radicals to alkenes - and experimental and theoretical perspective. *Angew. Chem. Int. Ed.*, 40:1340–1371, 2001.

[33] Davide Moscatelli, Marco Dossi, Carlo Cavallotti, and G. Storti. Density functional theory study of the addition reactions of carbon-centered radicals to alkenes. *J. Phys. Chem. A*, 40:1340–1371, 2011.

[34] Emmanuelle Boubour and Bruce Lennox. Insulating properties of self-assembled monolayers monitored by impedance spectroscopy. *Langmuir*, 16:4222–4228, 2000.

[35] Raluca Marcu, Stefania Rapino, Mirella Trinei, Giovanni Valenti, Massimo Marcaccio, Pier Giuseppe Pelicci, Francesco Paolucci, and Marco Giorgio. Electrochemical study of hydrogen peroxide formation in isolated mitochondria. *BIOELECTROCHEMISTRY*, 85:21–28, JUN 2012.

[36] JK Norskov, J Rossmeisl, A Logadottir, L Lindqvist, JR Kitchin, T Bligaard, and H Jonsson. Origin of the overpotential for oxygen reduction at a fuel-cell cathode. *JOURNAL OF PHYSICAL CHEMISTRY B*, 108(46):17886–17892, NOV 18 2004.

[37] Maria Campos, Wilai Siriwatcharapiboon, Robert J. Potter, and Sarah L. Horswell. Selectivity of cobalt-based catalysts towards hydrogen peroxide formation during the reduction of oxygen. *CATALYSIS TODAY*, 202:135–143, MAR 15 2013.

[38] Manas Pal and Vellaichamy Ganesan. Electrocatalytic activity of cobalt Schiff base complex immobilized silica materials to-

wards oxygen reduction and hydrazine oxidation. *CATALYSIS SCIENCE & TECHNOLOGY*, 2(11):2383–2388, NOV 2012.

[39] T Okada, S Gotou, M Yoshida, M Yuasa, T Hirose, and I Sekine. A comparative study of organic cobalt complex catalysts for oxygen reduction in polymer electrolyte fuel cells. *JOURNAL OF INORGANIC AND ORGANOMETALLIC POLYMERS*, 9(4):199–219, DEC 1999.

[40] Pingjie Wei and Hiroyoshi Tanabe. Synergy effects between single-walled carbon nanotubes and polypyrrole on the electrocatalysis of their composites for the oxygen reduction reaction. *CARBON*, 49(14):4877–4889, NOV 2011.

[41] Zheng Gong, Guoquan Zhang, and Song Wang. Electrochemical Reduction of Oxygen on Anthraquinone/Carbon Nanotubes Nanohybrid Modified. *JOURNAL OF CHEMISTRY*, 2013.

[42] JY Qu, S Yan, XH Qu, and SJ Dong. Electrocatalytic reduction of oxygen at multi-walled carbon nanotubes and cobalt porphyrin modified glassy carbon electrode. *ELECTROANALYSIS*, 16(17):1444–1450, SEP 2004.

[43] Barbara Kowalewska, Magdalena Skunik, Katarzyna Karnicka, Krzysztof Miecznikowski, Malgorzata Chojak, Grazyna Ginalska, Anna Belcarz, and Pawel J. Kulesza. Enhancement of bioelectrocatalytic oxygen reduction at the composite film of cobalt porphyrin immobilized within the carbon nanotube-supported peroxidase enzyme. *Electrochimica Acta*, 53(5):2408 – 2415, 2008.

[44] Yong Zhao, Kazuya Watanabe, and Kazuhito Hashimoto. Self-supporting oxygen reduction electrocatalysts made from a nitrogen-rich network polymer. *Journal of the American Chemical Society*, 134(48):19528–19531, 2012.

[45] Narita E., Lawson F., and Han K.N. Solubility of oxygen in aqueous electrolyte solutions. *Hydrometallurgy*, 10(1):21–37, 1983.

[46] Prabhpreet Singh, Giuseppe Lamanna, Cécilia Ménard-Moyonnd Francesca M. Toma, Elena Magnano, Federica Bondino, Maurizio Prato, Sandeep Verma, and Alberto Bianco. Formation of efficient catalytic silver nanoparticles on carbon nanotubes by adenine functionalization. *Angew. Chem. Int. Ed.*, 123:10067–10071, 2011.

[47] Ivar Kruusenberg, Nadezda Alexeyeva, Kaido Tammeveski, Jekaterina Kozlova, Leonard Matisen, Vaeino Sammelselg, Jose Solla-Gullon, and Juan M. Feliu. Effect of purification of carbon nanotubes on their electrocatalytic properties for oxygen reduction in acid solution. *CARBON*, 49(12):4031–4039, OCT 2011.

[48] Paulina Canete-Rosales, Valeria Ortega, Alejandro Alvarez-Lueje, Soledad Bollo, Monica Gonzalez, Alejandro Anson, and Maria Teresa Martinez. Influence of size and oxidative treatments of multi-walled carbon nanotubes on their electrocatalytic properties. *ELECTROCHIMICA ACTA*, 62:163–171, FEB 15 2012.

[49] Ivar Kruusenberg, Nadezda Alexeyeva, and Kaido Tammeveski. The ph-dependence of oxygen reduction on multi-walled carbon nanotube modified glassy carbon electrodes. *Carbon*, 47(3):651 – 658, 2009.

[50] Ren-Sheng Zhong, Yuan-Hang Qin, Dong-Fang Niu, Jing-Wei Tian, Xin-Sheng Zhang, Xin-Gui Zhou, Shi-Gang Sun, and Wei-Kang Yuan. Effect of carbon nanofiber surface functional groups on oxygen reduction in alkaline solution. *Journal of Power Sources*, 225(0):192 – 199, 2013.

[51] Kenji Matsubara and Keiko Waki. Oxygen reduction characteristics of bamboo-shaped, multi-walled carbon nanotubes without nitrogen in acid media. *Electrochimica Acta*, 55(28):9166 – 9173, 2010.

[52] Omar Israel Gonzalez-Pena, Thomas W. Chapman, Yunny Meas Vong, and Rene Antano-Lopez. Study of adsorption of citrate on Pt by CV and EQCM. *ELECTROCHIMICA ACTA*, 53(17):5549–5554, JUL 1 2008.

[53] Francesca M. Toma, Andrea Sartorel, Matteo Iurlo, Mauro Carraro, Pietro Parisse, Chiara Maccato, Stefania Rapino, Benito Rodriguez Gonzalez, Heinz Amenitsch, Da Tatiana Ros, Loredana Casalis, Andrea Goldoni, Massimo Marcaccio, Gianfranco Scorrano, Giacinto Scoles, Francesco Paolucci, Maurizio Prato, and Marcella Bonchio. Efficient water oxidation at carbon nanotube–polyoxometalate electrocatalytic interfaces. *Nat. Chem.*, 2:826–831, 2010.

[54] Andrea Sartorel, Pere Miro, Sophie Romain, Mauro Carraro, Gianfranco Scorrano, Marilena Di Valentin, Antoni Llobet, Carles Bo, and Marcella Bonchio. Water oxidation at a tetraruthenate core stabilized by polyoxometalate ligands: experimental and computational evidence to trace the competent intermediates. *J. Am. Chem. Soc.*, 131:16051–16053, 2009.

[55] Andrea Sartorel, Mauro Carraro, Gianfranco Scorrano, Rita De Zorzi, Silvano Geremia, Neal D. McDaniel, Stefan Bernhard, and Marcella Bonchio. Polyoxometalate embedding of a tetraruthenium(iv)-oxo-core by template-directed metalation of [gamma-$siw_{10}o_{36}$]$^{8-}$: a totally inorganic oxygen-evolving catalyst. *J. Am. Chem. Soc.*, 130:5006–5007, 2008.

[56] Gianluca Bernardini, Anthony G. Wedd, Chuan Zhao, and Alan M. Bond. Photochemical oxidation of water and reduction of polyoxometalate anions at interfaces of water with ionic liquids or diethylether. *PNAS*, 109:11552–11557, 2012.

[57] Chong-Yong Lee, Si-Xuan Guo, Aidan F. Murphy, Timothy McCormac, Jie Zhang, Alan M. Bond, Guibo Zhu, Craig L. Hill, and Yurii V. Geletii. Detailed electrochemical studies of the tetraruthenium polyoxometalate water oxidation catalyst in acidic media: identification of an extended oxidation series using fourier transformed alternating current voltammetry. *Inorg. Chem.*, 51:11521–11532, 2012.

This thesis and the graphics contained were created and elaborated using Open Source software

For more information on Open Source software visit:

opensource.org

www.fsf.org